ADDIS ABABA UNIVERSITY

ADDIS ABABA INSTITUTE OF TECHNOLOGY

SCHOOL OF CIVIL AND ENVIRONMENTAL ENGINEERING

Investigation of Shear Fatigue Behavior of Reinforced Concrete Beams Under Moving Load

A Thesis in Structural Engineering

By Noah Girma

January 16, 2020

Addis Ababa

A Thesis

Submitted in Partial Fulfillment of the Requirements for the Degree of Master of Science

The undersigned have examined the thesis entitled '**Investigation of Shear Fatigue Behavior of Reinforced Concrete Beams Under Moving Load'** presented by **Noah Girma**, a candidate for the degree of **Master of Science** and hereby certify that it is worthy of acceptance.

Dr. Ing. Adil Zekaria	_____	_____
Advisor	Signature	Date
Dr. Esayas Gebreyouhannes	_____	_____
Internal Examiner	Signature	Date
Dr. Abraham Gebre	_____	_____
External Examiner	Signature	Date
Dr. Ing. Mebruk Mohammed	_____	_____
Chair Person	Signature	Date

UNDERTAKING

I certify that research work titled “Investigation of Shear Fatigue Behavior of Reinforced Concrete Beams Under Moving Load” is my own work. The work has not been presented elsewhere for assessment. Where material has been used from other sources it has been properly acknowledged / referred.

Noah Girma

ABSTRACT

Reinforced concrete beams subjected to moving cyclic loads has a reduced fatigue life as compared to that of fixed-point pulsating loading. Moving loads has more damaging effect to the concrete, this might cause brittle shear failure.

In this study experimental and analytical investigation was conducted on six reinforced concrete beams without web reinforcements, to study the behavior of shear fatigue in reinforced concrete beams subjected to moving loads. One beam was made to fail monotonically to determine the static shear capacity. Three beams were subjected by a step wise moving load to 85%, 75% and 68% of the static shear capacity. The other two beams were subjected to a fixed-point pulsating load to 75% of the static shear capacity, but in different loading location (at midspan and at a location where the shear force to capacity ratio is maximum). Step wise moving load caused faster shear strength degradation compared to fixed pulsating load. Rate of increase in residual deflections with number of load cycles in step wise moving loads is higher compared to stationary cyclic loading which shows higher damage accumulation more than that of fixed pulsating load. Crack formation and propagation was monitored throughout the experimental programs by manually marking when new cracks formed. In fatigue loading the major diagonal cracks in beams are more horizontal than that of monotonic loading conditions. Depending on the amplitude of loading it is difficult for diagonal cracks to propagate into the compression zone in case of fatigue loading.

Key words: Step-wise moving load, fixed-point pulsating load, shear fatigue, RC beam

ACKNOWLEDGMENTS

I would like to express my gratitude to my advisor Dr. Adil Zekaria for the useful comments, remarks and engagement throughout the research period of this master thesis. Furthermore, I would like to thank Dr. Esayas Gebreyouhannes for introducing me the topic as well for the support on the way. Also, I would like to thank Addis Ababa Institute of Technology material laboratory staffs, who have willingly helped me during the experimental tests. I would like to thank my parents, friends and anyone who have supported me during this research. Last but not least I would like to thank God for giving me the strength and hope throughout the entire process.

TABLE OF CONTENTS

CONTENTS

UNDERTAKING ..... **III**

ABSTRACT ..... **IV**

ACKNOWLEDGMENTS ..... **V**

TABLE OF CONTENTS ..... **VI**

OF TABLES ..... **VIII**

LIST OF FIGURES ..... **IX**

CHAPTER 1 INTRODUCTION **1**

1.1 Background 1

1.2 Objective 2

1.3 Scope 2

1.4 Significance 2

1.5 Methodology 3

CHAPTER 2 LITREATURE REVIEW **4**

2.1 General Introduction 4

2.2 Shear fatigue behavior under cyclic loading 5

2.2.1 Gebreyouhannes et al. (2019) 5

2.2.2 Kawaguchi et al. (1990) 6

2.2.3 Chang and Kesler (1950) 7

2.2.4 Higai (1978) 9

2.2.5 Gebreyouhannes et al (2008) 10

2.2.6 Tsegereda Getachew (2018) 11

CHAPTER 3 EXPERIMENTAL PROGRAM **13**

3.1 Specimens 13

3.2 Materials 15

3.2.1 Concrete 15

3.2.2 Steel 16

3.3 Specimen fabrication 17
3.4 Test setup 19
3.5 Instrumentation 20
CHAPTER 4 FEM ANALYSIS 23
4.1 About the software 23
4.2 Specimens 23
4.3 Materials 23
4.4 Modeling 25
4.5 Support condition and loading 25
CHAPTER 5 RESULTS AND DISCUSSIONS 27
5.1 Results 27
5.1.1 Test summaries 27
5.1.2 Experimental Results 36
5.1.3 Analytical results 40
5.2 Discussion 44
5.2.1 Comparison in response of experimental beams 44
5.2.2 Comparison in response of analytical beams 49
5.2.3 Comparison between experimental and analytical results 51
5.2.4 Diagonal crack pattern 54
5.2.5 S-N curve 56
CHAPTER 6 CONCLUSION AND RECCOMENDATION 58
6.1 Conclusion 58
6.2 Recommendation 59
REFERENCES 60
ANNEX 62

LIST OF TABLES

Table 3-1: Specimen designation.....14
Table 3-2: 28th day strength of cube samples. 15
Table 3-3: mix proportions of concrete 15
Table 3-4: mechanical properties of reinforcement bars 17
Table 4-1: specimen designation and description.....23
Table 4-2: Mechanical Properties of Concrete 24
Table 4-3: Mechanical property of reinforcement bar.....24
Table 5-1: Summary of experimental result 27
Table 5.2: summary of analytical results.....41

LIST OF FIGURES

Figure 2.1: various fatigue failures encountered by Chang & Kesler 8
Figure 2.2: fatigue of the longitudinal reinforcement in the constant moment region with no inclined cracks. 9
Figure 2.3: Failure mechanism in a reinforced concrete beam with no web reinforcement 10
Figure 2.4: loading set-up and crack pattern. 11
Figure 3.1: beam Specimen and loading setup 14
Figure 3.2: compression testing machine 16
Figure 3.3: reinforcement cage 16
Figure 3.4 tensile strength testing machine 17
Figure 3.5: Formwork 18
Figure 3.6: Curing of casted specimen 18
Figure 3.7: test setup 19
Figure 3.8: point of load application for the step-wise moving load 20
Figure 3.9: hydraulic jack and load cell 20
Figure 3.10: data logger 21
Figure 3.11: linear variable displacement transducers (LVDT) installed under the beam 21
Figure 3.12: linear variable displacement transducers (LVDT) installed at the back 22
Figure 4.1: Finite element mesh for monotonic beam (MB) 26
Figure 4.2: Reinforcement cage for all beams 26
Figure 5.1: MB after failure 28
Figure 5.2: FCB75 after failure (front side) 29
Figure 5.3: FCB after failure (rear side) 29
Figure 5.4: FCB75c after failure 31
Figure 5.5: Diagonal cracks in both halves of the specimen MCB85 32
Figure 5.6: MCB85 after failure 32
Figure 5.7: diagonal cracks propagating in to compression zone in both halves of MCB75 33
Figure 5.8: MCB75 after failure 34
Figure 5.9: diagonal crack that formed in the 2nd loading in specimen MCB68 35
Figure 5.10: MCB68 after failure 36

Figure 5.11: load deflection diagram for specimen MB 36
Figure 5.12: load deflection diagram for specimen FCB75 37
Figure 5.13: load deflection diagram for specimen FCB75c 37
Figure 5.14: load deflection diagram for specimen MCB85 38
Figure 5.15: load deflection diagram for specimen MCB75 38
Figure 5.16: load deflection diagram for specimen MCB68 39
Figure 5.17: midspan deflection history of FCB75 & MCB75 39
Figure 5.18: midspan deflection history of MCB85, MCB75 & MCB68 40
Figure 5.19: strain contour output of A-MB 40
Figure 5.20: strain contour output A-MCB85 in load step 47 41
Figure 5.21: load deflection diagram of specimen A-MB 41
Figure 5.22: load deflection diagram of specimen A-MCB85 42
Figure 5.23: load deflection diagram of specimen A-MCB75 42
Figure 5.24: load deflection diagram of specimen A-MCB68 43
Figure 5.25: load deflection diagram of specimen A-FCB75 43
Figure 5.26: comparison between MB and MCB85 44
Figure 5.27: comparison between MB and MCB75 45
Figure 5.28: comparison between MCB68 and MB 45
Figure 5.29: comparison between FCB75 and MB 46
Figure 5.30: comparison between FCB75Cand MB 47
Figure 5.31: Midspan deflection versus number of cycles for MCB75 47
Figure 5.32: Midspan deflection versus number of cycles for FCB75 48
Figure 5.33: comparison between A-MB and A-MCB85 49
Figure 5.34: comparison between A-MB and A-MCB75 49
Figure 5.35: comparison between A-MCB68 and A-MB 50
Figure 5.36: comparison between A-FCB75 and A-MB 51
Figure 5.37: comparison between MB and A-MB 51
Figure 5.38: comparison between MCB85 and A-MCB85 52
Figure 5.39: comparison between MCB75 and A-MCB75 52
Figure 5.40: comparison between MCB68 and A-MCB68 53
Figure 5.41: comparison between FCB75 and A-FCB75 53
Figure 5.42: Diagonal crack paths of specimen MB, MCB85, MCB75 and MCB68 54
Figure 5.43: Diagonal crack path of specimen MB 55
Figure 5.44: Diagonal crack paths of specimen MCB85 55

Figure 5.45: Diagonal crack paths of specimen MCB75 55
Figure 5.46: Diagonal crack paths of specimen MCB68 56
Figure 5.47: deflection-number of cycle relation 56
Figure 5.48: S-N diagram for moving cyclic loaded beams 57

CHAPTER 1 INTRODUCTION

1.1 Background

Concrete is a composite material which consists of three components: the cement matrix, the aggregate, and the matrix-aggregate interface. This cement-matrix is the composite's weakest zone. Attenuation in a material or part that is subjected to cyclic loading leads to an increase in concentration of stress around the micro-cracks and eventually to fracture. The forces needed to achieve a fracture are typically much less than the forces necessary for monotonic loading. It is caused by progressive, irreversible internal structural changes in the material, which may result in propagation of micro-cracks until the formation of main macro-cracks. The macro-cracks lead to reduction of the cross-section and in turn to an even greater concentration of stress which leads to fracture, CEB (1988).

The perception of fatigue is very important both from an economic point of view and from a safety point of view of the structures. Modern structures have become lighter and thinner, resulting in higher stress concentrations and higher proportions of different load conditions relative to total loads. Examples of concrete structures exposed to cyclic loading that causes fatigue include highways, airfields and bridges.

Damage due to fatigue can be divided into various groups depending on the conditions of loading, as well as other factors e.g. environment. One can describe the various fatigue forms as follows:

High-cycle fatigue: When the material needs a failure of more than 10^3-10^4 cycles then one claims the material is subjected to high cyclic fatigue. The deterioration process is related to load frequencies.

Low-cycle fatigue: This type of fatigue is defined by a number to failure which is less than 10^3-10^4. Low cycle fatigue is also related to high loading amplitudes resulting in loss of material stiffness.

Thermal fatigue is the product of temperature gradient that varies with time in such a way that cyclic stresses are generated in a material specimen. In other words, the thermal fatigue is obtained when fast alternating heating and cooling cycles occur. Crack

propagation will occur due to expansions and extensions and the fatigue mechanism will be significantly accelerated by increasing temperature variation. Power-pipe lines can be listed as an example of structures where thermal fatigue occurs.

Corrosion fatigue: For the material specimen that is subjected to both cyclic loading and corrosive environment, the failure may occur at lower loads and after a shorter time than for pure cyclic loading. This type of failure is denoted as fatigue from corrosion. (Ameen et al. 2006)

Structural fatigue can be described as the process of damage buildup due to time-varying stress application. An incremental amount of damage happens each time a load cycle is applied. In fact, this damage is cumulative, and accumulation persists until the failure occurs. If fatigue cracks are found early then it might be possible to repair them. If not detected and repaired correctly, the effects could be catastrophic failures. Bridges are one of the examples where similar situation may arise.

1.2 Objective

The objective of this research work is to investigate the shear fatigue behavior of reinforced concrete beams without web reinforcements subjected to both moving cyclic loads and fixed-point pulsating load.

1.3 Scope

Reinforcement fatigue is ignored in both analytical and experimental tests. This is because the main target is to investigate the fatigue degradation of concrete. This research is only limited to reinforced concrete beams without shear reinforcements.

1.4 Significance

Fatigue damage can occur in many bridges, which are exposed to millions of load cycles during service life. The performance degradation in the shear capacity of bridge girders under repeated service loads is not quantified during the design process. Thus, understanding fatigue in reinforced concrete beams could be of great importance.

1.5 Methodology

Experimentally and analytically investigate reinforced concrete beams subjected to step wise moving load and fixed-point pulsating load. Mode of failure, nature of crack formation and propagation and relation between number of cycles to failure and maximum stress for the step-wise moving load will be the focus of the study.

CHAPTER 2 LITREATURE REVIEW

2.1 General Introduction

Material fatigue happens when they are exposed to rapidly fluctuating and cyclic stresses. Material failure is usually caused by fatigue at stress levels much lower than the yield strength of a material for a static load. Small faults or discontinuities arise internally or on the surface of the body. As a consequence, cracks can grow under cyclic loading due to plastic deformation at these flaws, even if the normal stress applied is lower than the elastic limit. As the crack length rises, the intact portion of the structure cannot withstand the load applied due to the decreased area of stress resistance. This causes a very rapid crack growth which results in an abrupt material failure. (Naik, 1993)

There are two types of fatigue loading which can lead to different mechanisms of failure. They are called Low-cycle fatigue and High-cycle fatigue. Low-cycle fatigue means the load is applied for a fairly limited number of cycles at high stress levels, whereas the high-cycle fatigue refers to a large number of cycles at lower stresses. Low cycle fatigue is essential for earthquake loaded structures.(Ahsan, 2016)

Metal fatigue has been under study for over a century, and extensive information has been accumulated about it. Yet the study on concrete fatigue is not only far less radical, but far less conclusive. However, many concrete structures such as highway pavements, highway bridges, rail bridges, airport pavements and bridges, maritime structures, etc. are subject to dynamic loads. Fatigue strength data of concrete materials and other materials used in such structures are required to obtain their safe, efficient and economical design.

While fatigue has not proved to be a problem for concrete structures to date, as structures are becoming smaller, traffic volumes are rising, axle loads are rising and traffic speed limits are higher, the margin of reserve strength is gradually decreasing.

2.2 Shear fatigue behavior under cyclic loading

Shear fatigue behavior of reinforced concrete structures without shear reinforcement is a very complex process involving a great number of variables. Chang and Kesler first identified this process from their comprehensive experimental campaign on beams that were subjected to four-point bending fatigue. The first stage of the process involves the creation of a diagonal crack at the shear span on an existing flexural crack. This shear crack then propagates to the compression zone on the one side, and to the support running roughly parallel to the longitudinal reinforcement on the other side. Fatigue failures occur when diagonal crack propagation has reduced the depth of the compression zone such that the compressive force acting on it cannot be resisted. This failure mode was called shear-compression fatigue by Chang and Kesler. Furthermore, some experiments also showed that the diagonal crack could grow absolutely instantaneously. Chang and Kesler called this second failure mode a diagonal-cracking fatigue failure. (Gallego et al., 2014)

2.2.1 Gebreyouhannes et al. (2019)

This paper deals with the shear fatigue mechanism in reinforced concrete beams which are subject to pulsating and moving loads. Experimental study was done on three shear critical reinforced concrete beams of size (155mm x 300mm x 2200mm). The key goals of the research were focused to the sequence of crack formation and crack propagation, load deflection responses under loading and the progress of beam deflection during the loading cycles. Experimental analysis was done by applying a stationary pulsating and a moving load on reinforced concrete beams, and results were related with an identical beam subjected to a monotonic load. In order to evaluate the static capacity, the first beam was tested for failure under monotonic loading, the other two beams were subjected to repeated loading lower than their static capacity. Of these two beams, one was subjected to a stationary pulsating load at midspan while the other was subjected to a step-wise moving load along the span. The study employed an automated crack mapping system (digital image correlation) during testing to provide proof of crack formation and damage evolution. Test results showed that the step-wise moving load had a much more destructive effect on the concrete, decreasing the beam's shear fatigue life by nearly two orders of magnitude, from 1600 cycles to 51 load passages (255 cycles) only. From the response of the beam that was subjected to the mid span pulsating load it was seen that residual deflections were cumulative with increasing load cycles, indicating buildup of damage

inside the concrete. There has also been a steady decline in overall beam stiffness, with increased load cycles. The beam subjected to the moving load had a greater increase in beam deflection with increasing load cycles/passages, confirming the damage experienced by the beam than the other two beams. The authors suggest that this damaging effect is due to the fact that moving load has the effect of regularly altering the principal stress orientation which, in turn, has the effect of accelerating fracture and damage process within the concrete.(Gebreyouhannes & Suryanto, 2019)

2.2.2 Kawaguchi et al. (1990)

This paper investigated the effect of a running load on the fatigue behavior of reinforced concrete beams. Experiment was conducted on beams with size 50mm wide by 80mm high and with 600mm, 800mm, 1000mm and 1200mm long at Nihon University. Authors wanted to understand the effect of running load in detail on the process of crack development and failure type. Tests were done on reinforced concrete beams of four different span lengths to observe the fatigue behavior under the running load. These beams were subjected to stationary loads and running load. The static test was made by applying a repetitive fatigue loading on a fixed point of a beam. For the case of the running load beams were set on a movable bed, which was driven back and forth by an air piston. The load was transferred via a caster onto a beam between the two supports. The caster had a steel wheel with solid rubber tire. On the static tests most of the beams experienced vertical flexural cracks initiated under the load and diagonal crack developed later on one side of the beams. Fractures took place along the diagonal cracks. Deflection of the beams tended to increase suddenly near the failure. This showed that brittle shear fracture of beams developed abruptly. On the running load tests all beams failed in shear. Fatigue strength of beams that were subjected to the running load were remarkably lower than the beams under a repeated load on a fixed point. Process of crack development were almost the same for all four kinds of spans. Authors suggest that reduction of the fatigue strength of beams under the running load were due to alternative stress induced by transferring a load had a significant role. Authors derived an equation to predict the fatigue failure of a beam. Cycles to fatigue failure of beams distributed so widely that it was almost impossible to predict the fatigue life of each beam through S-N curve. It was observed in the experiments that cracks and total deflection grew faster near fatigue failure. This fast growth of cracks

and deflection took place at around 80% of fatigue life, then they proposed the simple formula for prediction of the fatigue life once the fast growth of cracks is observed. (Kawaguchi et al., 1990)

2.2.3 Chang and Kesler (1950)

In the 1950's Chang and Kesler performed one of the earliest studies in shear fatigue of reinforced concrete beams. The goal was to create clear and adequate expressions for the static strength of beam shear failure, and to assess the strength of reinforced concrete beams under repeated loading without web reinforcement. The rest of this article will concern their research on fatigue loading.

Chang and Kesler tested 39 specimens that had a 4 x 6 in. long, simply supported, and loaded at the one-third points with equal loads. The shear span-to-depth ratio for all specimens was 3.53. They considered concrete strength, percentage of longitudinal reinforcement, and maximum applied shear as their primary variables. The tests were continued to failure or ten million cycles at which time a static strength test was performed. Information related to initial diagonal cracking and final failure of the beams, if they did not fail when diagonal cracking occurred, was obtained. Chang and Kesler observed three types of fatigue failure:

1. Fatigue of longitudinal reinforcement in the constant moment region with inclined cracking present (figure 2.1a).
2. Diagonal cracking (figure 2.1b).
3. Shear compression (figure 2.1c).

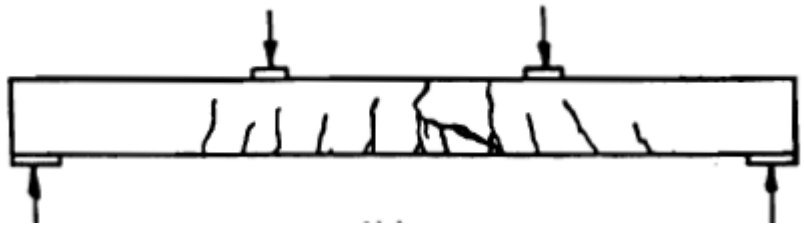

(a)

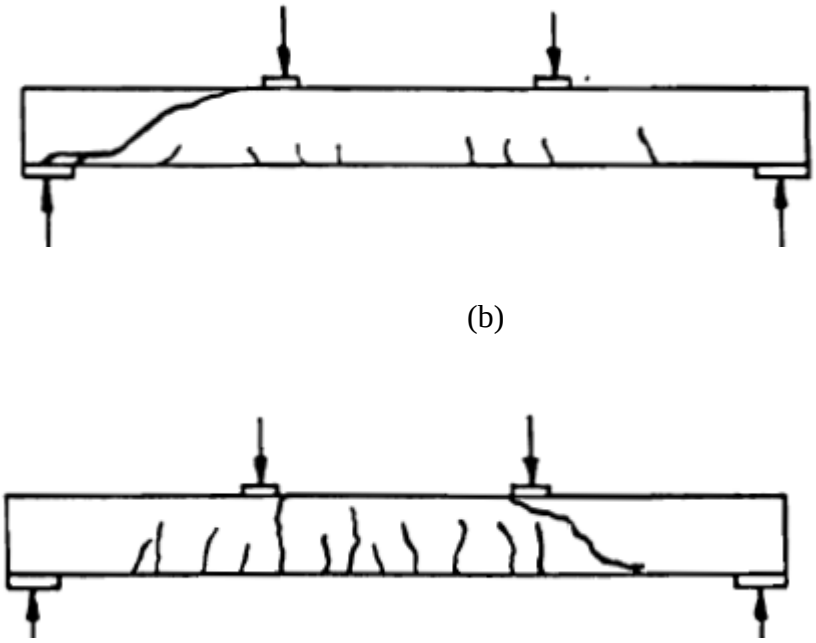

(b)

(c)

Figure 2.1: various fatigue failures encountered by Chang & Kesler

Important conclusions reached in the study included:

1. The fatigue strength of the type of specimens tested was influenced by the percentage of steel and concrete strength, to the same extent as static strength.
2. For fatigue loading up to 100,000 cycles, the cracking load was reduced at a more rapid rate than the ultimate failure load.
3. If a beam did not crack diagonally under fatigue loading, neither the diagonal tension cracking load, nor the ultimate moment capacity were affected. If a beam was cracked diagonally under fatigue loading but did not fail, the static load capacity was not affected.

In another study by Chang and Kesler 8, they tested 25 more specimens of identical cross section and loading arrangement. This time they lowered the amount of longitudinal reinforcement tensile reinforcement in order to study the complicated fatigue behavior of a reinforced concrete beam that would fail in flexure at a static load only slightly less than that which would produce a shear failure. They had three control specimens to determine the ultimate static load and to verify that flexural behavior would dominate during static

load tests. The fatigue specimens exhibited the same three types of failure as the previous study except that in addition, fatigue of the longitudinal reinforcement in the constant moment region with no inclined cracks was possible as shown in the figure bellow. In general, low amplitude repeated loads resulted in flexural fatigue failure, while high amplitude repeated loads resulted in a shear fatigue failure. Chang and Kesler were probably the first researchers to demonstrate that a reinforced concrete beam, which would fail in flexure when loaded monotonically, could fail in shear when subjected to fatigue loads. This was an extremely important discovery because it implied that fatigue loading could change the limit state for design. (Bachman et al., 1987)

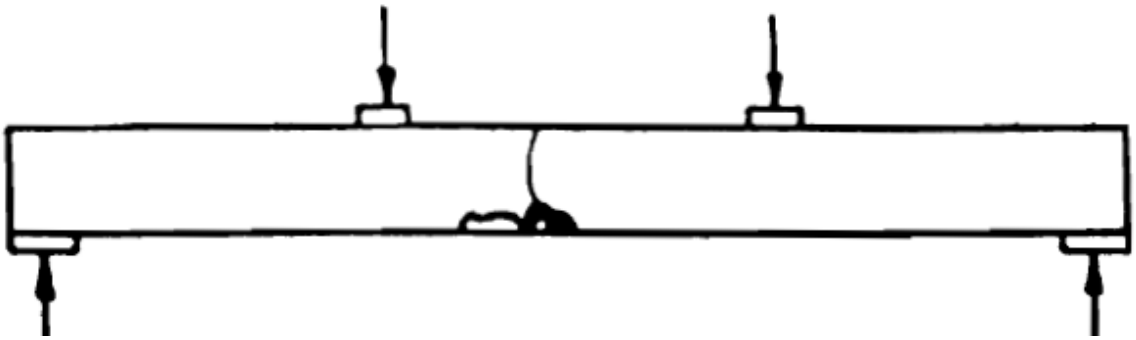

Figure 2.2: fatigue of the longitudinal reinforcement in the constant moment region with no inclined cracks.

2.2.4 Higai (1978)

In 1978 Higai tested 130 rectangular and T-shaped reinforced concrete sections to determine their shear response when subjected to moving loads and fatigue loads. He studied the effect of shear span-to-depth ratio and its effect on the fatigue failure mechanism. It was observed for beams with no web reinforcement and a small a/d ratio that the beam would not fail immediately upon initiation of inclined cracks, while at some larger a/d ratio the same beam would fail immediately upon initiation of inclined cracking. He proposed that at low a/d ratios the arch-mechanism failure load, instead of diagonal cracking, controlled the behavior of the beam. As a result, the beam would not fail upon initiation of diagonal cracks. At high a/d ratios, the diagonal cracking load instead of the arch mechanism failure load-controlled failure. He proposed that under fatigue loading, the diagonal cracking load was

reduced by a certain amount at a given number of cycles. Therefore, beam with an a/d ratio such that it would fail at initiation of a diagonal cracking under static load, would not fail but would develop arch action under fatigue load. this concept is shown graphically in fig 5. Higai also discussed the well-known phenomenon of increased shear strength near supports or concentrated loads. He proposed that for design purposes it would be better to consider a reduction in applied shear force near supports or concentrated loads. He suggested a form for a relationship to describe such a reduction. (Higai, 1978)

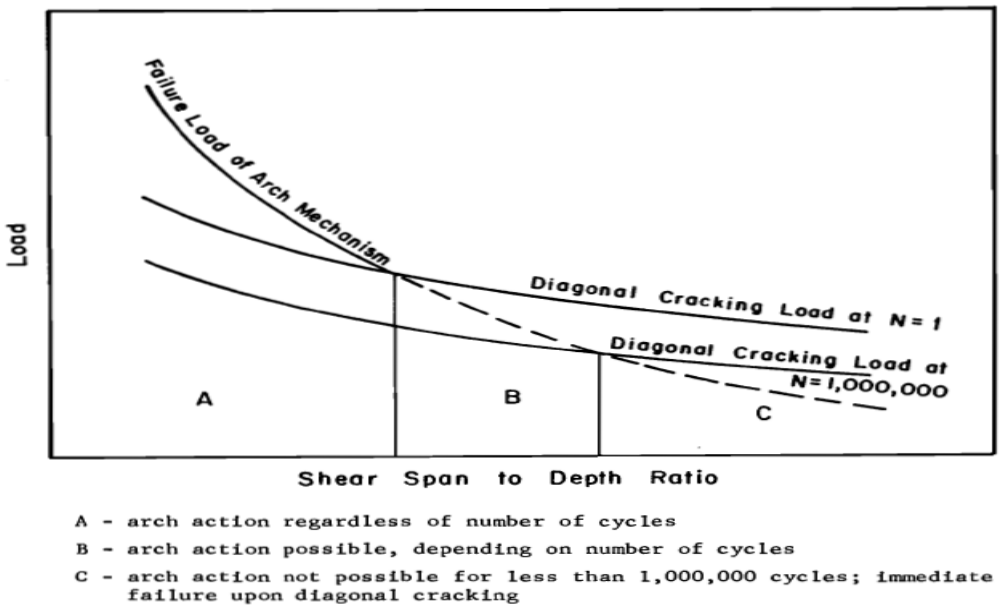

Figure 2.3: Failure mechanism in a reinforced concrete beam with no web reinforcement

2.2.5 Gebreyouhannes et al (2008)

Investigation on Shear Fatigue of reinforced concrete Beams exposed to Fixed Point cyclic and Moving Loads was done in Japan in 2008 by Esayas Gebreyouhannes, Nobuhiro Chijiwa, Chikako Fujiyama and Koichi Maekawa. The fatigue performance of reinforced concrete beams exposed to moving loads was experimentally investigated as shown in the figure below. Analytical inspection was made on the shear fatigue performance of reinforced concrete beams exposed to moving loads based on strain path and time dependent fatigue constitutive models. Moving load is found to cause dramatic drop in fatigue life of beams as related to that of the fixed Point cyclic load both in the experiment and analysis.

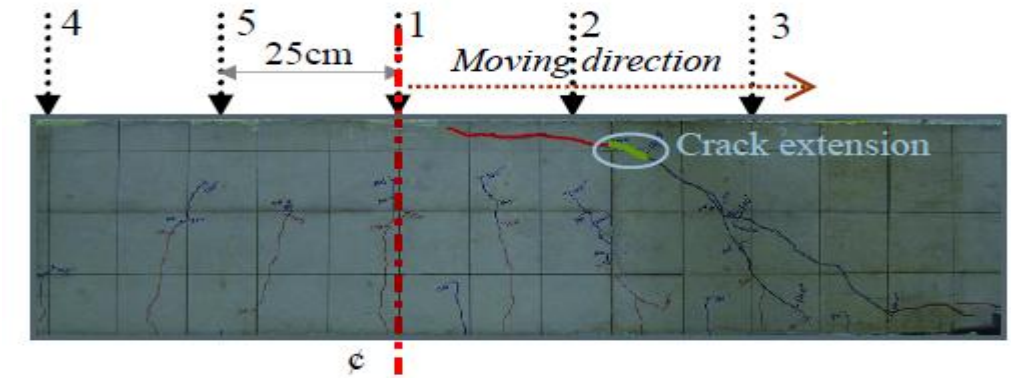

Figure 2.4: loading set-up and crack pattern.

The fatigue life of RC beams under moving load is greatly reduced, and is 2-3 orders lower than that of fixed Point cyclic load. This huge reduction in the fatigue life of RC beams under moving load is due to the joint effects of stress/displacement reversal and variation in shear force to capacity ratio. Based on the analysis, a simple relation for the prediction of fatigue life under moving load is proposed on the basis of the standard shear fatigue relation of JSCE, for practical use. Asymmetric type of loading is found to significantly reduce the fatigue life as compared to central-axis based loading. (Gebreyouhannes et al., 2008)

2.2.6 Tsegereda Getachew (2018)

Research on the fatigue behavior of Shear critical reinforced concrete beams in Addis Ababa institute of technology was conducted in 2018 by Tsegereda Getachew. Her purpose was to investigate the performance of shear critical beams under one sided cyclic loading, to investigate the performance of beams without web reinforcement under low-cycle fatigue loading and to quantify shear strength degradation of RC beams with number of cycles for low-cycle fatigue analysis.

Six experimental beams were tested under constant amplitude fatigue loading until failure and analytical investigation were also conducted using FEA software comprising a strain path and time-dependent fatigue constitutive model.

Conclusions reached in the study were: -

1) Provision of shear reinforcement greatly enhances the shear capacity of RC beams and also improves their performance under fatigue loading.
2) For members with shear reinforcement, the load deflection response measured under monotonic loading provided an excellent envelope for load deflection response under fixed amplitude fatigue loading.
3) Both concrete and the stirrups showed cyclic material softening.
4) One-sided cyclic loading of shear critical slender beams causes shear strength degradation with respect to their expected monotonic capacity.
5) It is possible that fatigue loading has a favorable effect on RC beams by altering diagonal crack path and enhancing the shear capacity of the beams.
6) The equation which was developed for calculating the fatigue shear strength of shear-critical beams was in close agreement with S-N curves proposed by different researchers for beams without shear reinforcement and plain concrete. (Getachew, 2018)

CHAPTER 3 EXPERIMENTAL PROGRAM

This chapter describes the experimental program on the shear fatigue behavior of reinforced concrete beams. The experiment was conducted at the Construction Materials Laboratory, Addis Ababa Institute of Technology. The test consisted of six simply supported reinforced concrete beams without shear reinforcement, which were subjected to three types of loadings (monotonic, step wise moving cyclic load and fixed cyclic load). The main variable is the type of loading. Monotonic load was applied on the reference beam while step-wise moving cyclic load and fixed cyclic load were applied to the test beams. Other parameters have remained as constant as possible. Shear failure was assured by providing high strength longitudinal reinforcement bar and by not using web reinforcements. Shear failure was further confirmed by calculating and comparing the flexural and shear capacity of the beams. All beams have a similar cross section, longitudinal reinforcement, and web reinforcement ratio. The shear capacity of all the beam specimens was calculated according to Eurocode 2 (EN1992-1-1, 2004).

3.1 Specimens

Reduction in fatigue life of reinforced concrete beams subjected to step-wise moving loads is experimentally investigated. The experimental program consists of 6 simply supported RC beam specimens with rectangular cross section and constant breadth (b) and Depth (D) of 200 mm and 250 mm respectively and length 2000mm. Figure 3.1 shows details and reinforcement arrangement of the specimens. All beams do not have a web reinforcement in the clear span. To prevent anchorage failure stirrups were provided out of the effective length.

The experimental and analytical beams are designated according to the type of loading and amplitude of fatigue as a percentage of the ultimate capacity of the monotonic beam.

Table 3-1: Specimen designation

Specimen Designation	Meaning	Analytical Designation
MB	Monotonic beam	A-MB
MCB85	Moving cyclic beam 85% of the ultimate capacity	A-MCB85
MCB75	Moving cyclic beam 75% of the ultimate capacity	A-MCB75
MCB68	Moving cyclic beam 68% of the ultimate capacity	A-MCB68
FCB75	Fixed cyclic beam 75% of the ultimate capacity	A-FCB75
FCB75c	Fixed cyclic beam 75% of the ultimate capacity loaded at critical location	A-FCB75c

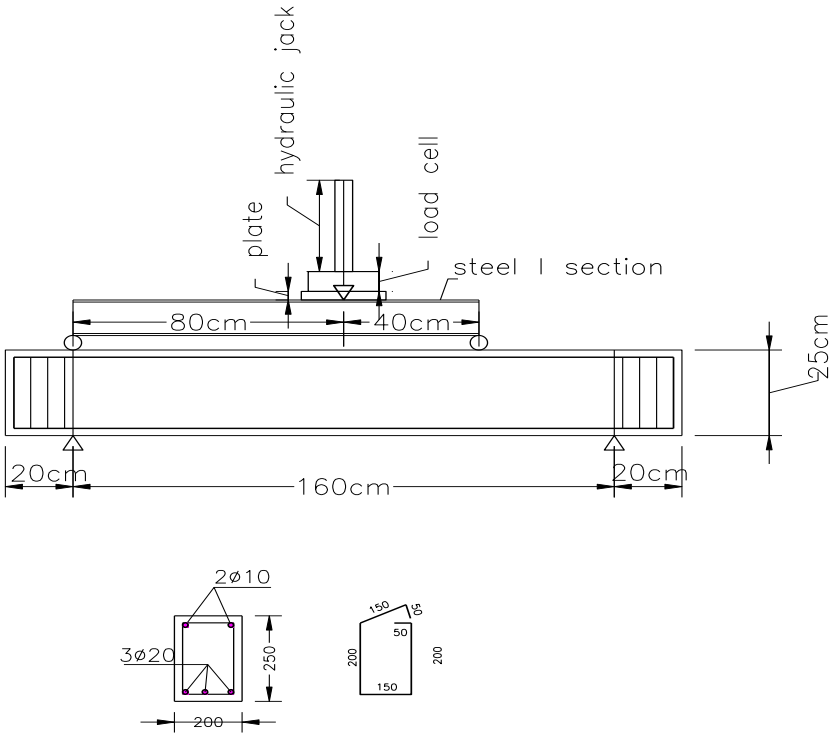

Figure 3.1: beam Specimen and loading setup

3.2 Materials

3.2.1 Concrete

All specimens were casted in a formwork made of plywood using cast in situ concrete. During the casting process of concrete, 3 samples of concrete cylinders were prepared in a cylinder of diameter 100mm and height 300 mm. and 6 samples concrete cubes of 150mm were casted. 3 cube samples from each beam were tested after 28days of casting. The rest 3 cubes and 3-cylinder samples were tested on the testing dates of the respective beams. In the mix proportions of concrete, ordinary Portland cement was used and water-cement ratio was kept at 0.579.

Table 3-2: 28th day strength of cube samples.

samples	Compressive Strength (MPa)			
	Cube 1	Cube 2	Cube 3	Average
MB	37.32	31.94	34.58	34.61
FCB75	34.26	33.01	34.9	34.06
FCB75c	36.14	34.37	37.93	36.14
MCB85	42.71	40.53	41.62	41.62
MCB68	41.21	40.61	35.47	39.09
MCB75	24.89	38.42	35.94	33.08

The concrete mix was designed according to ACI and binary method. The weight method was employed for this thesis. Mix proportions of concrete was as shown bellow

Table 3-3: mix proportions of concrete

Average cubic strength	33MPa
OPC cement	328.152kg/m3
Maximum aggregate size	25mm
water	190kg/m3
Coarse aggregate	999.591kg/m3
Fine aggregate	791.304kg/m3
Water cement ratio	0.579

Cube samples were tested using a compression testing machine as shown in the figure bellow.

Figure 3.2: compression testing machine

3.2.2 Steel

Longitudinal reinforcements were used to ensure shear failure. For the bottom reinforcements 20mm diameter rebars were installed and 10mm rebars were installed for the top longitudinal reinforcements. 8mm diameter deformed bars were used at the edges of the beam outside the effective length to avoid anchorage failure.

Figure 3.3: reinforcement cage

Tests were conducted on the reinforcement bars to determine its tensile strength and other mechanical properties.

Figure 3.4 tensile strength testing machine

Table 3-4: mechanical properties of reinforcement bars

specimen	Average diameter(mm)	Yield strength (MPa)	Fracture strength (MPa)	Ultimate strain εu (‰)
8	7.64	567.44	723.84	120
10	9.475	569.01	734.31	150
20	19.12	617.12	732.23	180

3.3 Specimen fabrication

First reinforcement cage was manufactured by a professional rebar worker. Web reinforcements of 8mm diameter bars were tied on to the longitudinal bars outside the effective length of the beam. Then it was installed into a ply wood formwork. The formwork was made by plywood and it was stiffened at three positions throughout its length to avoid bulging of forms during casting of concrete. After the formwork was

prepared the reinforcement cages were placed inside by maintaining a concrete clear cover of 25mm on all sides.

Figure 3.5: Formwork

Concrete was casted in the AAiT compound by using a mechanical mixer and electric vibrator. The beam and the samples are cured in the same manner by covering them with wet cotton material and to reduce rate of evaporation polyethylene sheet was used on top of the wet cotton. Casted specimens and curing of specimens are shown bellow

Figure 3.6: Curing of casted specimen

3.4 Test setup

The tests were conducted on steel plates with two roller supports on each side of the steel plates. The beams were then rested on these two supports and load was applied manually by a hydraulic jack with a maximum capacity of 300KN.

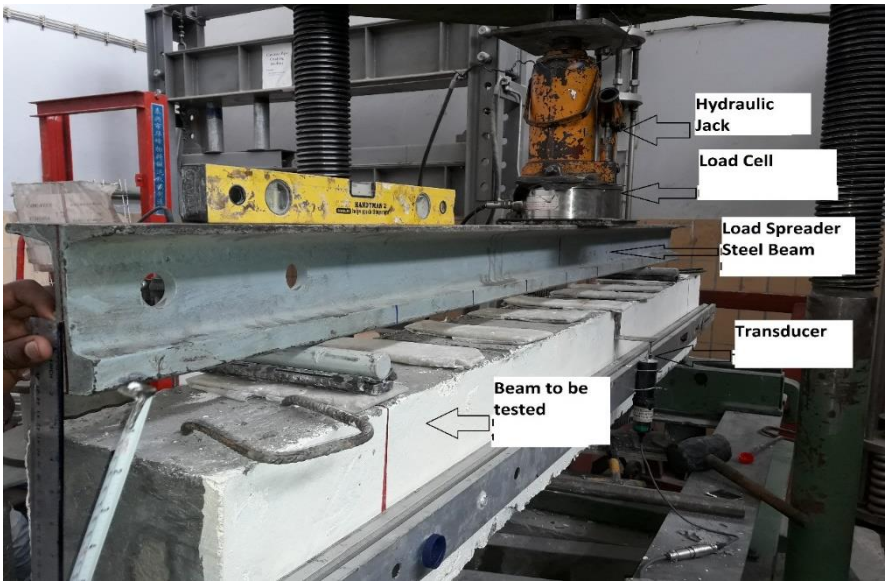

Figure 3.7: test setup

To perform the moving load a stiff steel I-section with a depth of 120mm was used as a spreader beam as shown in Figure 3.7. Below this beam, two roller supports were installed to transfer the loads. One full passage comprised seven load steps. In load step 1, one of the roller supports was positioned directly above the right support and the other at load point A. The beam was then loaded up to a certain percentage of its maximum capacity before being fully unloaded. The spreader beam was then lifted to allow the roller support on the left to be shifted to load point B. The beam was then subjected to same load cycle of amplitude. the same technique was employed again to apply load on to point C. To perform load step 4, the spreader beam was first lifted and the roller support was moved to load point D while the other roller support was taken off temporarily, then load was directly applied to the midspan. This continued with load step 5,6 & 7 essentially mirrored load step 3,2 & 1 at load points E, F & G. In the fixed cyclic loading case, the spreader beam was not necessary to perform loading, the hydraulic jack was made to rest on a very elastic plate directly on the point of loading then stationary cyclic load was applied.

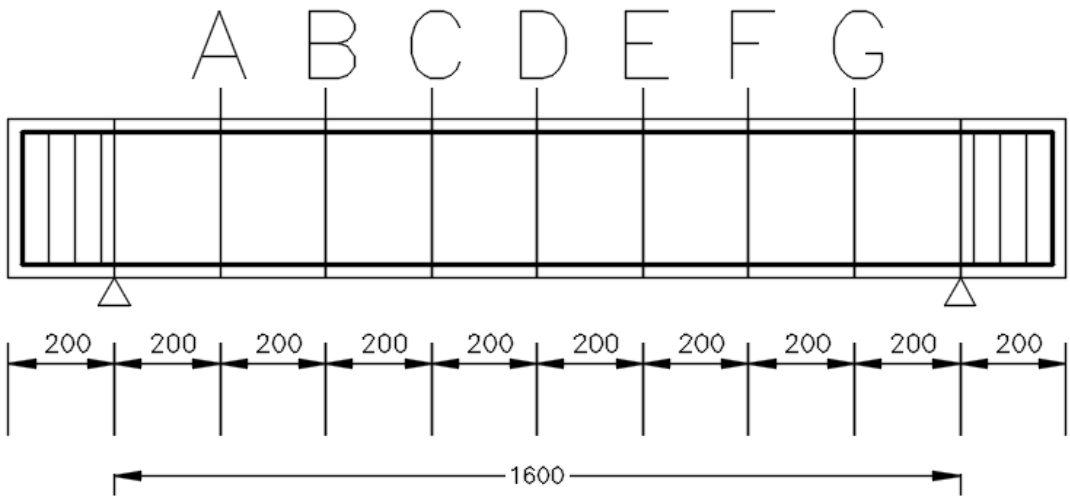

Figure 3.8: point of load application for the step-wise moving load

3.5 Instrumentation

The main instruments used on the tests are the hydraulic jack which is used for applying the load, the load cell to measure the applied load, the linear variable transducers to measure the displacement of the beam upon loading and the data logger which is used for recording the load with its corresponding displacement of the beam.

Figure 3.9: hydraulic jack and load cell

Figure 3.10: data logger

Figure 3.11: linear variable displacement transducers (LVDT) installed under the beam

Figure 3.12: linear variable displacement transducers (LVDT) installed at the back

Two linear variable displacement transducers were employed during the tests. Although the reading from the transducer which was placed under the beam is a little exaggerated, its increment in displacement from cycle to cycle is close to the transducer which was placed on the back side of the beam.

CHAPTER 4 FEM ANALYSIS

4.1 About the software

For the analytical simulation of this study, the DuCOM-COM3D system which is developed in the university of Tokyo is used. This is a multi-scale analysis code that links the thermo-chemo-physics platforms DuCOM and COM3D. DuCOM-COM3D is capable of predicting the change in concrete material properties. The long-term structural response under actual ambient conditions can be predicted in a realistic manner.

4.2 Specimens

Three-dimensional nonlinear finite element analysis was carried out for 6 specimens with identical mechanical properties to the experimental beams. The specimens were categorized in three groups based on loading types to study the effect of fatigue loading in shear failure of reinforced concrete beam. Table 4-1 shows the specimen designation, cross-sectional property and reinforcement detailing of the 6 specimens.

Specimen designation	Cylindrical compressive strength f_{cm} (MPa)	tensile strength of concrete, f_{ctm} (MPa)	Type of loading
A-MB	28.41	2.64	monotonic
A-MCB85	33.2	2.54	moving one sided cyclic
A-MCB75	31.69	2.3	moving one-sided cyclic
A-MCB68	35.2	2.25	moving one-sided cyclic
A-FCB75	32.34	2.54	fixed one-sided cyclic at midspan
A-FCB75c	30.71	2.50	fixed one sided cyclic at critical location

Table 4-1: specimen designation and description

All the beams are modeled identical to the respective experimental beams. This was done in order to use the outputs from the analytical simulation as a verification for the experimental results.

4.3 Materials

The tensile strength, the cylindrical compressive strength and modulus of elasticity of concrete were computed according to Eurocode 2 (EN1992-1-1:2004). During the

experiment cubic samples were prepared to determine the concrete strength of each beams. For the analytical software in DuCOM-COM3D cylindrical strength of concrete was needed as an input for material database. Mean cylindrical strength was determined by multiplying the cube strength a variable coefficient from Table 3.1 of Eurocode 2. The modulus of elasticity of the concrete was computed according to equation 4.1. The tensile strength of the concrete was taken directly from the splitting tensile strength.

$$E_{cm} = 22\left[\frac{f_{cm}}{10}\right]^{0.3} \qquad (4.1)$$

Table 4-2: Mechanical Properties of Concrete

specimens	A-MB	A-MCB85	A-MCB75	A-MCB68	A-FCB75	A-FCB75c
Initial stiffness (GPa)	30.1	31.58	31.11	32.13	31.3	30.8
Compressive strength (MPa)	28.41	33.2	31.69	35.2	32.34	30.71
Tensile Strength (MPa)	2.64	2.54	2.3	2.25	2.54	2.50
Poison's ratio	0.2	0.2	0.2	0.2	0.2	0.2
Unit Weight (Kg/m^3)	2356.54	2410.86	2381.23	2392.59	2455.31	2390.62

Tensile strength test was done for the reinforcements used in the beams. Detail property of the reinforcing steel bars are described in Table 4-3.

Table 4-3: Mechanical property of reinforcement bar

	Bottom longitudinal bar	Top reinforcement	Stirrup for anchorage
Initial stiffness (Gpa)	200	200	200
Yield strength (Mpa)	617.12	569.01	567.44
Tension rupture strength (Mpa)	732.23	734.31	723.84
Tension rupture strain	0.18	0.15	0.12
Poisson ratio	0.2	0.2	0.2
Unit weight (KN/m^3)	78	78	78

4.4 Modeling

The analysis was performed using the multi-directional fixed crack FE framework. All steel bars were modeled as embedded smeared reinforcement inside the elements. Concrete elements without steel bars were modeled as plain concrete element. Concrete with steel reinforcement was modeled as RC elements characterized by tension stiffening. Loading plates and support bearings were modeled as elastic elements characterized by unyielding behavior.

4.5 Support condition and loading

The beams were simply support with 1.6m clear distance between the supports. Elastic bearings were used at the support and at the point of load application. For specimen A-MB to capture the post peak behavior of the beams, a displacement-controlled analysis was performed by applying a downward displacement of 0.02 cm per minute for 50 load steps at the mid span. For the rest of the beams force-based fatigue loading was applied. For specimen A-FCB75 and A-FCB75c The input file was manipulated by applying a progressive magnification factor on the loading data based on the direct path integral scheme to reduce runtime. (Maekawa et al., 2006)

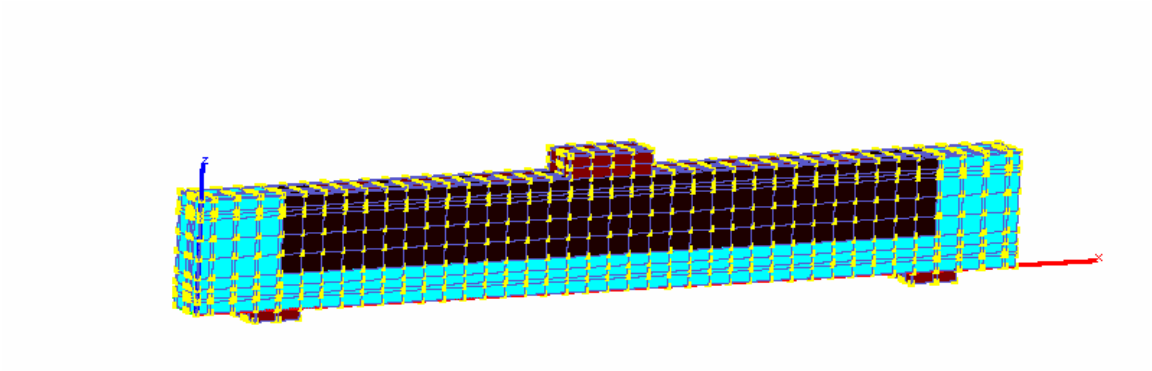

Figure 4.1: Finite element mesh for monotonic beam (MB)

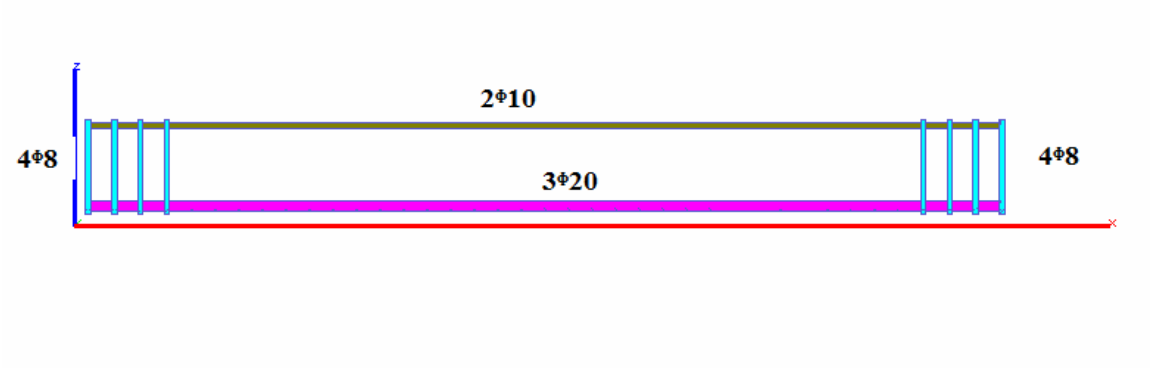

Figure 4.2: Reinforcement cage for all beams

CHAPTER 5 RESULTS AND DISCUSSIONS

5.1 Results

5.1.1 Test summaries

All experimental beams failed in a brittle manner. Failure was governed by the diagonal shear. Diagonal cracks propagated to the point of load application and to the support without anchorage failure. Splitting cracks along the longitudinal reinforcements were observed after the peak load.

Table 5-1: Summary of experimental result

Specimen	Cube Compressive Strength (MPa)	Cracking Load (KN)	Maximum Load (KN)	Number of Loading Points (n)
FCB75	39.17	87	146	1000+monotonic
FCB75c	45.64	82	216	1000+monotonic
MB	35.39	59	132.55	monotonic
MCB85	38.63	79	112.6	24
MCB75	39.48	86	99.4	213
MCB68	42.89	86.67	90	165

5.1.1.1 Monotonic beam (MB)

This beam was used to determine the monotonic shear capacity of the beams. Since all of the beams were casted with a material from similar source the beams are assumed to have a similar strength. This beam has an a/d of 3.86 and a concrete cubic compressive strength of 35.4MPa. After loading started, first flexural crack was observed at a load level of 59KN followed by other small flexural cracks beneath the loading point. Following the formation of the flexural cracks, a major diagonal shear crack developed and became visible at a load level of 132.55KN. The beam failed in shear, in a brittle manner.

Figure 5.1: MB after failure

5.1.1.2 FCB75

Testing was done by applying a fixed-point pulsating load (one sided cyclic loading) at the mid-span after 53days of casting. Specimen FCB75 was loaded up to 75% of its maximum capacity by a stationary pulsating load. It took three and half days to complete the test.

On the first loading cycle vertical flexural cracks developed near mid-span. Further loading cycles produced more flexural cracks that extended towards the point of load application in each cycle. But these cracks didn't widen throughout the test. Cracks tend to get wider when the beam is loaded and the cracks immediately closes after the beam is unloaded. After the first cycle this beam displayed almost a constant deflection with increasing number of cycles. The fixed-point pulsating load continued up to the 1000 cycle. After the 1000 cycles it was decided to load the beam monotonically since it's hard to continue cyclic loading manually until the beam fails. The beam was loaded monotonically and inclined crack formed very suddenly and was associated with the shear flexural cracks that formed due to the fatigue loading. Failure was sudden and occurred soon after inclined cracking. The beam failed in shear with a maximum load of 146.06KN in a brittle manner. The maximum load carried by this beam exceeded the control beam maximum capacity by 10.2%. This increase in shear capacity after fatigue loading was also observed in a previous research. (Getachew, 2018).

Figure 5.2: FCB75 after failure (front side)

Figure 5.3: FCB after failure (rear side)

5.1.1.3 FCB75c

Stress ratio varies with the movement of the load. According to Niwa's Equation for shear design of beams. The maximum stress ratio occurs at some distance away from the center. Fatigue at this point is more critical than at the center. The Niwa equation is used for diagonal cracking load. The predicted value calculated using the design equation is expressed as V_c. The Niwa equation is the basis of the shear capacity equation in the JSCE standard specification for design and construction of concrete structures. And it has been

confirmed as highly accurate with regard to normal strength materials and concentrated loadings. (Maekawa & Mishima, 2002).

$$\frac{V_C}{bd} = 0.2 * \sqrt[3]{f_c'} * \sqrt[3]{100\rho} * \sqrt[4]{1000/d} * \left(0.75 + \frac{1.4}{a/d}\right), \qquad \sqrt[3]{f_c'} \leq 3.6$$

Where, V_C is a diagonal cracking load (KN), f_c' is compressive strength as obtained with a cylinder test (N/mm^2), ρ is main tensile reinforcement ratio, b is member width (mm), d is effective depth (mm), and a is shear span (mm).

Using the above equation, the maximum shear force to capacity ratio was found to be 0.49m away from the support. Specimen FCB75c was used to test that fatigue at this point would be critical. Testing was done by applying a fixed-point pulsating load (one sided cyclic loading) at 0.31m away from midspan to the left support, after 64 days of casting. This beam was loaded up to 75% of its maximum capacity by a pulsating load. It took three days to reach 1000 cycles and after that the beam was made to fail monotonically. It was planned to show that fatigue at this point was critical but since the load range is small 1000 cycles were reached without a significant sign of failure. On the first loading cycle small flexural cracks started around the loading point and extended towards the point of load application in each cycle. Shear flexure cracks started developing on both sides of point of load application. After the first cycle this beam displayed almost a constant deflection with increasing number of cycles. Cracks tend to get wider when the beam is loaded and the cracks immediately closes after the beam is unloaded like the previous beam. The fixed-point pulsating load continued up to the 1000 cycle. Then the beam was loaded monotonically and inclined crack formed very suddenly and was not associated with the shear flexural cracks that formed due to the fatigue loading. Failure was sudden and occurred soon after inclined cracking. The beam failed in shear with a maximum load of 216.34KN in a brittle manner. Unfortunately, it failed on the side which was least expected. This is due to a significant reserve strength in the beam due to arch action. The maximum load carried by this beam exceeded the control beam maximum capacity by 63.2%.

Figure 5.4: FCB75c after failure

5.1.1.4 MCB85

MCB85 was tested under one-side cyclic loading 33 days later from casting. This beam was subjected to a cyclic step-wise moving loads with 85% percent of its maximum capacity. The first loading is applied at an offset distance of 20 cm to the right of the left support (loading point A) with amplitude of 112.7KN. In the second loading, at an offset distance of 40 cm from the left support (loading point B), formation of diagonal cracking is observed. In the third loading (loading point C) the, diagonal crack formed during the second loading, was extended. During the fourth loading (mid span) only flexural cracks occurred. In the fifth loading (loading point E) most of the flexural cracks extended. During the sixth loading (40 cm to the right of mid span) formation of diagonal cracking is observed on this half of the beam. Until the 18th loading there was always an extension of existing cracks. In the 18th loading the diagonal crack formed during the 6th loading showed an appreciable extension to the point of load application (mid span) by propagating into the compression zone and it also extended to the support by developing a splitting crack along the longitudinal reinforcement. Lastly, the beam failed in shear during the 24th loading, which is applied at loading point C (20 cm to the left of the midspan). The already extended diagonal crack propagated towards loading point C and the beam failed at a load of 91.78KN.

Figure 5.5: Diagonal cracks in both halves of the specimen MCB85

Figure 5.6: MCB85 after failure

5.1.1.5 MCB75

MCB75 was tested under one-side cyclic loading 48 days later from casting. This beam was subjected to a cyclic step-wise moving loads with 75% percent of its maximum capacity. The first loading is applied at an offset distance of 20 cm to the right of the left support with amplitude of 99.4KN. In the second loading, at an offset distance of 40 cm from the left support, only flexural cracks occurred. In the third loading (at point C), new

flexural cracks occurred beneath the loading point. During the fourth loading (mid span) other flexural cracks occurred. In the fifth and sixth loadings flexural cracks developed in this half of the beam. During the 85th loading (60 cm to the left of mid span) formation of diagonal cracking is observed on this half of the beam. The flexural crack formed in the 5th loading extended into diagonal crack on the other half of the beam. Until the beam failed there was always an extension of existing cracks.

During the 208th loading (20 cm to the right of mid span) new diagonal crack suddenly occurred at a load of 96.8KN. And it was on the most damaged half of the beam. This indicates that, damage tends to accumulate on the previously damaged part due to other loading points. The new crack propagated into the compression zone and it also extended to the support by developing a splitting crack. Lastly, the beam failed in shear in the 213th loading point, which is applied at loading point C (20 cm to the left of the midspan). The diagonal crack that formed in the 208th loading propagated towards loading point C and the beam failed at a load of 93.44KN. New inclined crack also occurred towards load point C. but the beam failed along the previous winded diagonal crack. This beam failed after 30 passages, and this result do not deviate much from a previous study on RC beam subjected to a moving cyclic load with 75% of its capacity, the beam failed at 51 passages but loading points here were only at five different locations along the beam not seven as in specimen MCB75. (Gebreyouhannes & Suryanto, 2019)

Figure 5.7: diagonal cracks propagating in to compression zone in both halves of MCB75

Figure 5.8: MCB75 after failure

5.1.1.6 MCB68

MCB68 was tested under one-side cyclic loading 41 days later from casting. At first it was planned to test the beam in a cyclic step-wise moving loads with 75% percent of its maximum capacity. The first loading was applied at an offset distance of 20 cm to the right of the left support (point A) with amplitude of 99.4KN. In the second loading, at an offset distance of 40 cm from the left support, when the load reached 90KN formation of an early diagonal crack which propagated into the compression zone was observed. This early crack was unexpected and it was evident if the amplitude of the load is to continue to be at 99.4KN the beam would have failed early and it wouldn't give us enough data to observe the progress of damage under moving load. so, it was decided to decrease the amplitude of the load to 90KN which caused the crack, to be the load. Making the amplitude to be 68% of the maximum capacity.

In the 3rd loading, flexural cracks occurred beneath the loading point and the diagonal crack that formed in the 2nd loading extended to the top of the compression zone. During the fourth loading (mid span) other flexural cracks occurred. In the fifth and sixth loadings flexural cracks developed in this half of the beam. Throughout the span extensive flexural cracks developed up to the last loading. Formation of diagonal cracking was also observed on the other half of the beam, but this crack was not wide as that of the first diagonal crack on the other half of the beam. New flexural crack formed and also there was extensions of existing flexural cracks until the last loading.

During the 165th loading (20 cm to the left of the mid span) new diagonal crack suddenly occurred at a load of 82.4KN. And it was on the most damaged half of the beam. This indicates that, damage tends to accumulate on the previously damaged part due to other loading points. The new crack propagated into the compression zone and it also extended to the support by developing a splitting crack (bond crack). Lastly, the beam failed in shear in this 165th loading, which is applied at loading point C (20 cm to the left of the midspan). The diagonal crack that formed in the 2nd loading propagated towards loading point B and the beam failed at a load of 86.4KN. New inclined crack also occurred towards load point C. But the beam failed along the diagonal crack that formed during the second loading.

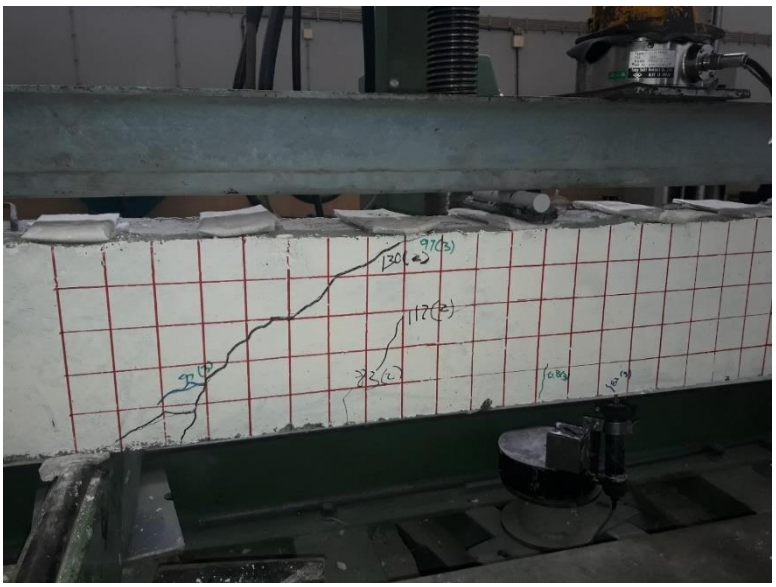

Figure 5.9: diagonal crack that formed in the 2nd loading in specimen MCB68

Figure 5.10: MCB68 after failure

5.1.2 Experimental Results

5.1.2.1 Load deflection curves

Load deflection diagrams of all beams are presented below.

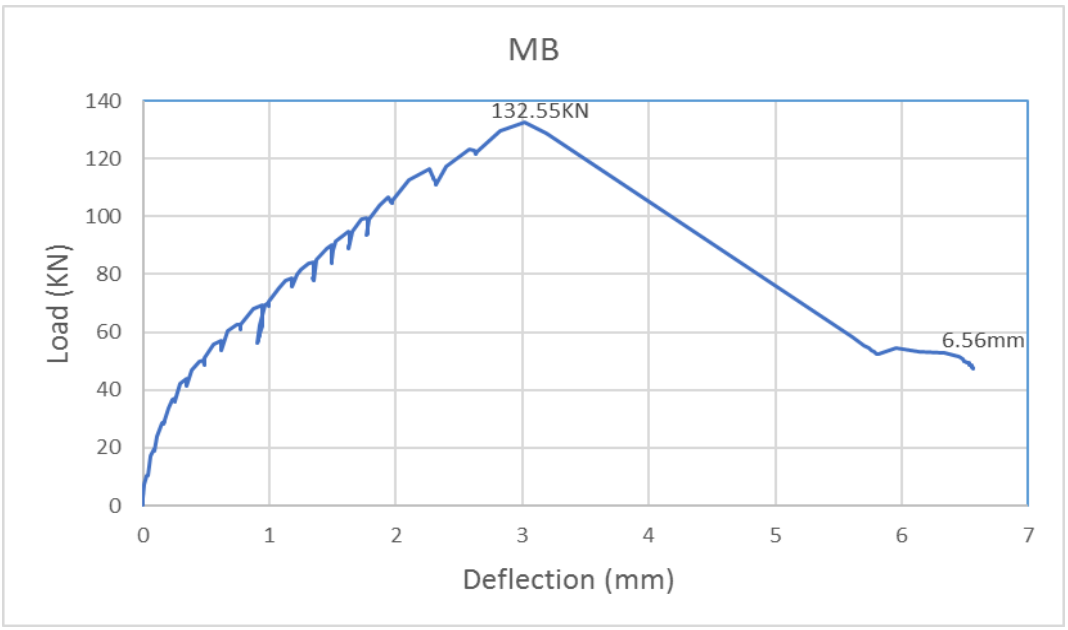

Figure 5.11: load deflection diagram for specimen MB

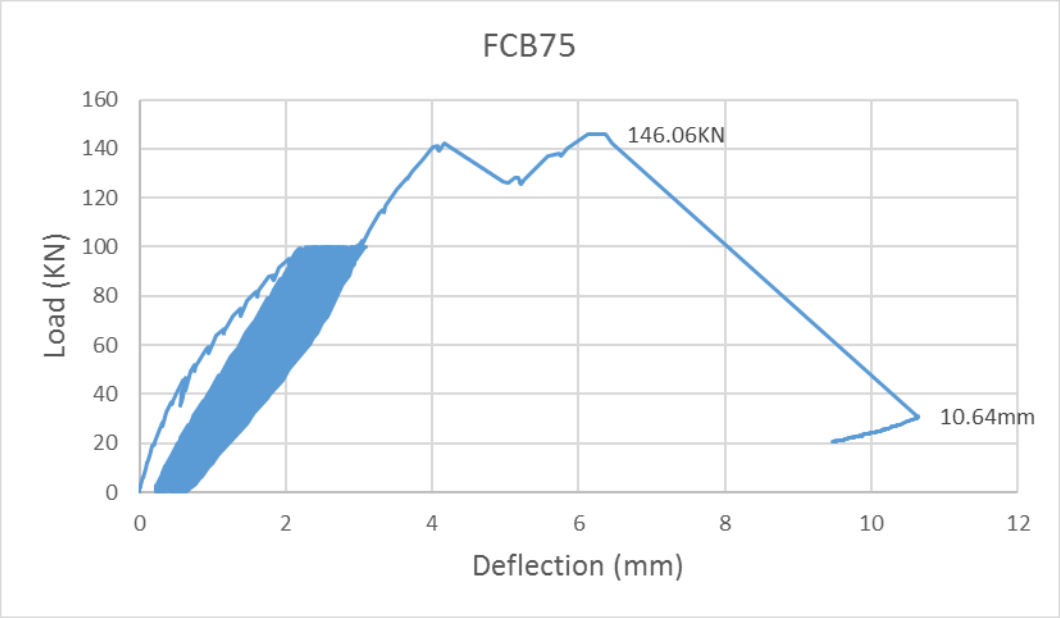

Figure 5.12: load deflection diagram for specimen FCB75

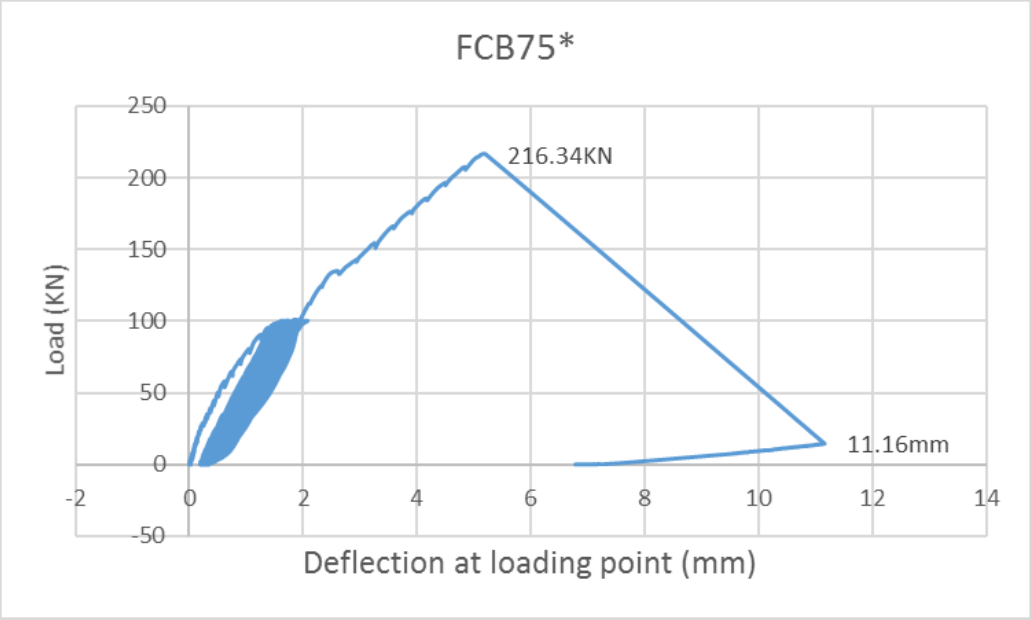

Figure 5.13: load deflection diagram for specimen FCB75c

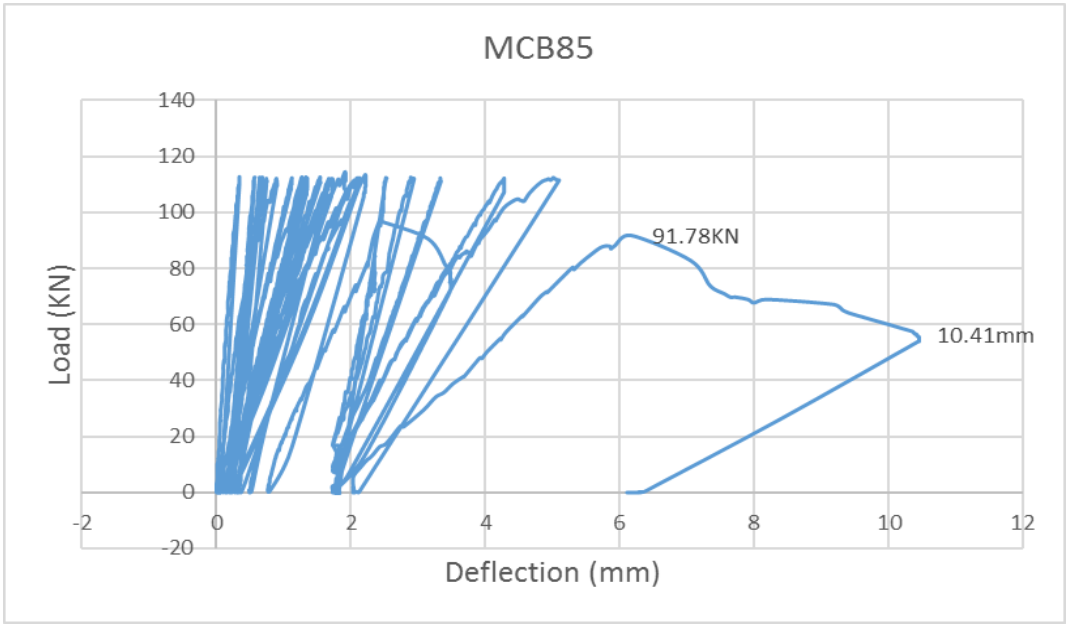

Figure 5.14: load deflection diagram for specimen MCB85

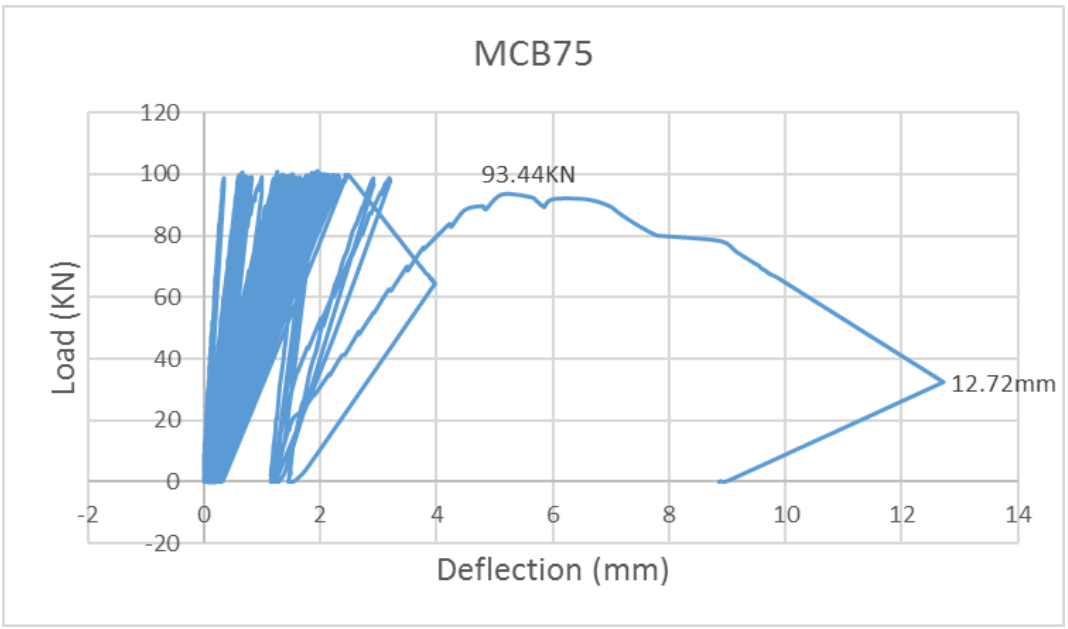

Figure 5.15: load deflection diagram for specimen MCB75

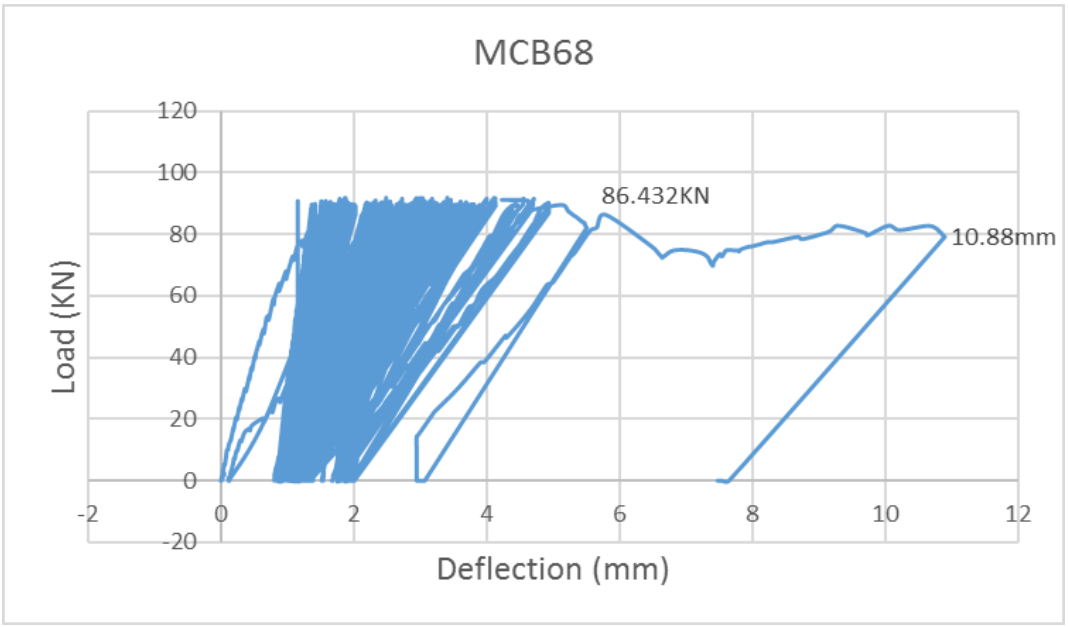

Figure 5.16: load deflection diagram for specimen MCB68

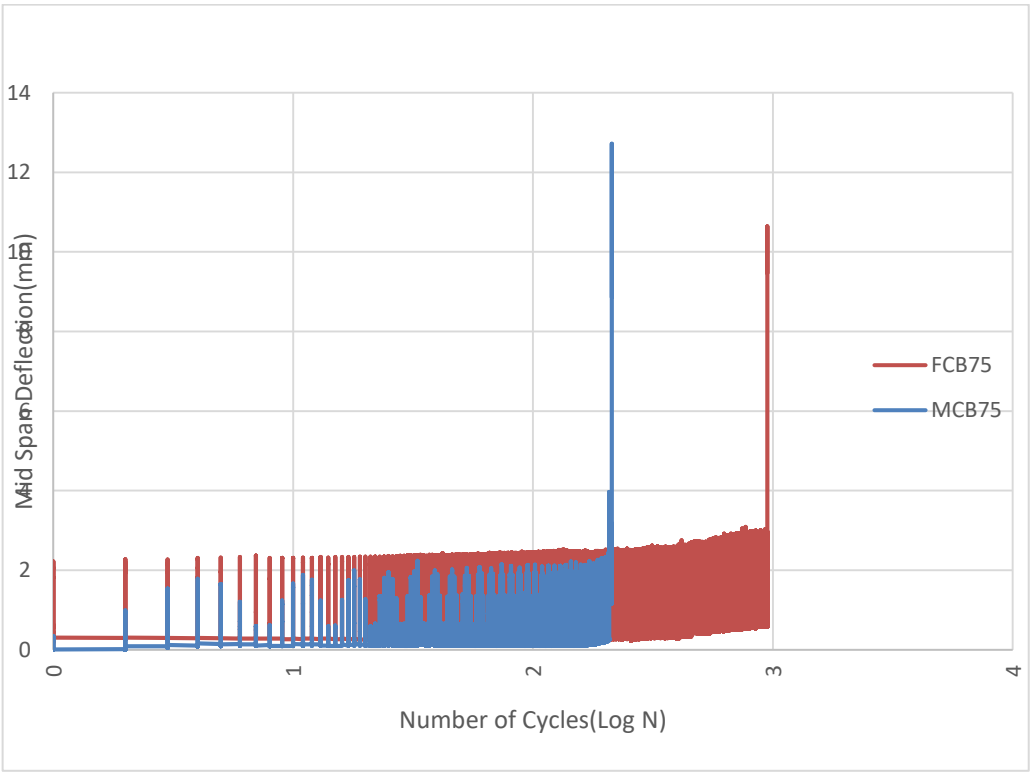

Figure 5.17: midspan deflection history of FCB75 & MCB75

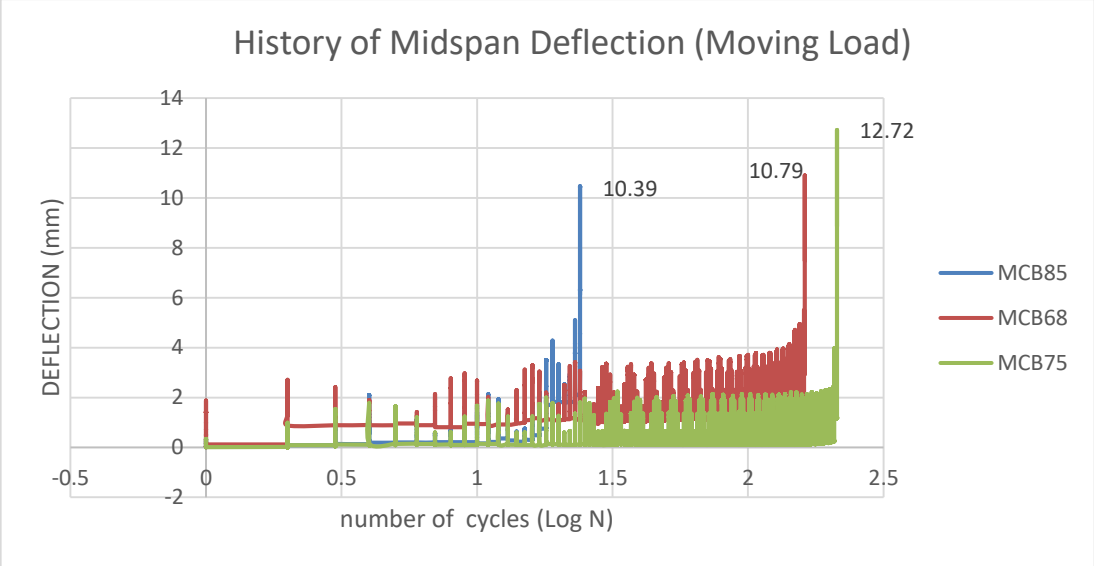

Figure 5.18: midspan deflection history of MCB85, MCB75 & MCB68

5.1.3 Analytical results

All analytical beams failed in shear as can be seen from load deflection curves and the strain contour. Diagonal cracks propagated to the point of load application and to the support without anchorage failure as it can be shown in the figures bellow. Force-based approach was used for fatigue analysis while monotonic simulation was displacement controlled.

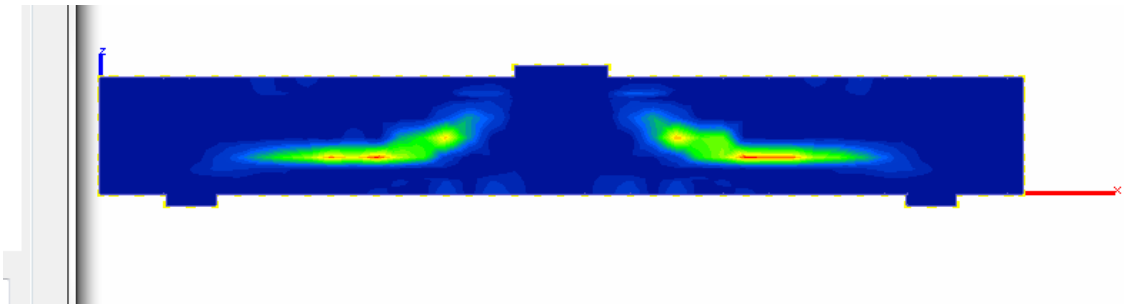

Figure 5.19: strain contour output of A-MB

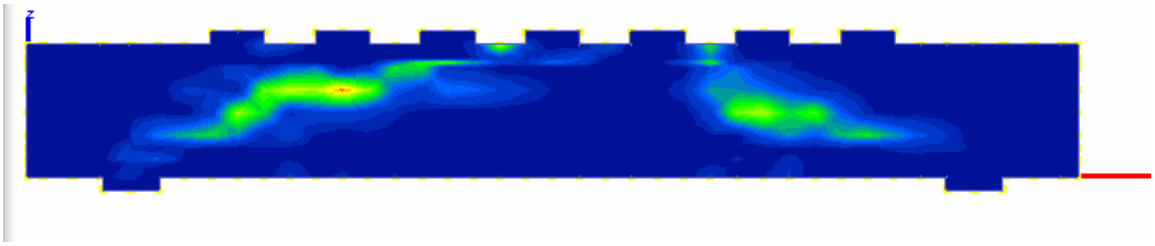

Figure 5.20: strain contour output A-MCB85 in load step 47

Table 5.2: summary of analytical results

Specimen	Cylindrical Compressive strength	Maximum Load P_{max} (KN)	Mid-span deflection at maximum load (mm)	Life cycle (n)
A-MB	28.4	128	2.8	monotonic
A-MCB85	33.31	108.74	20.34	26
A-MCB75	31.69	95.9	15.47	120
A-MCB68	35.28	87.04	10.88	195
A-FCB75	32.34	95.9	22	1413

5.1.3.1 Load deflection curves

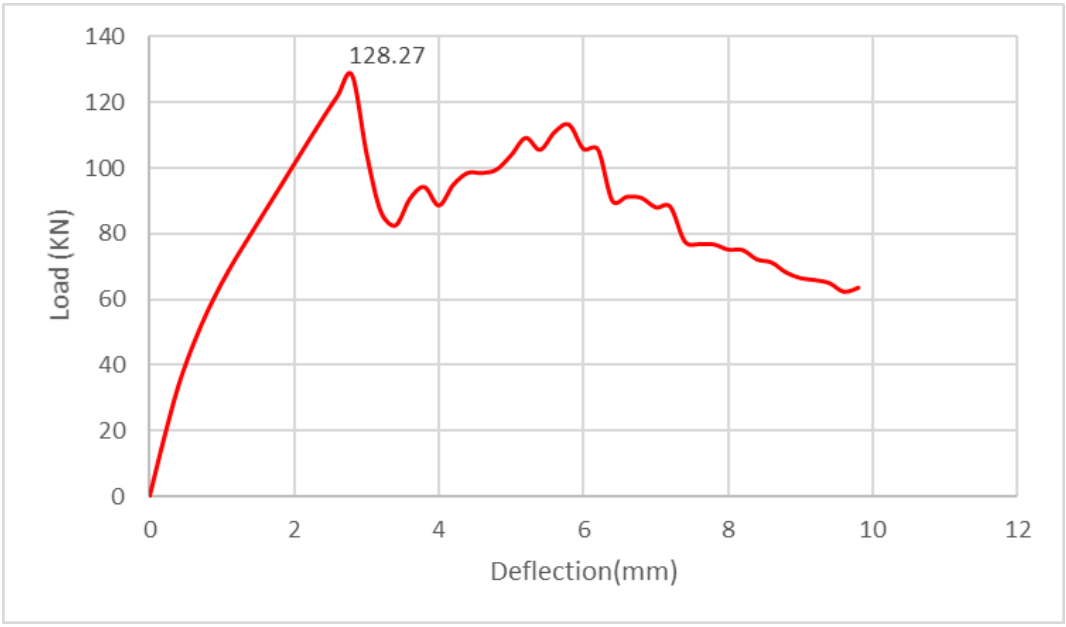

Figure 5.21: load deflection diagram of specimen A-MB

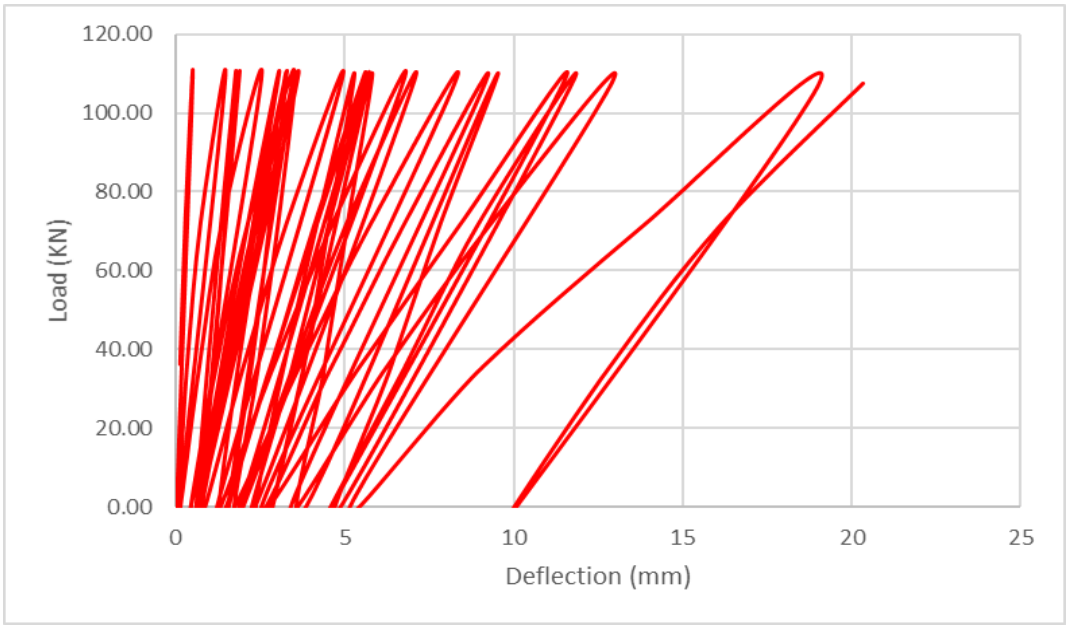

Figure 5.22: load deflection diagram of specimen A-MCB85

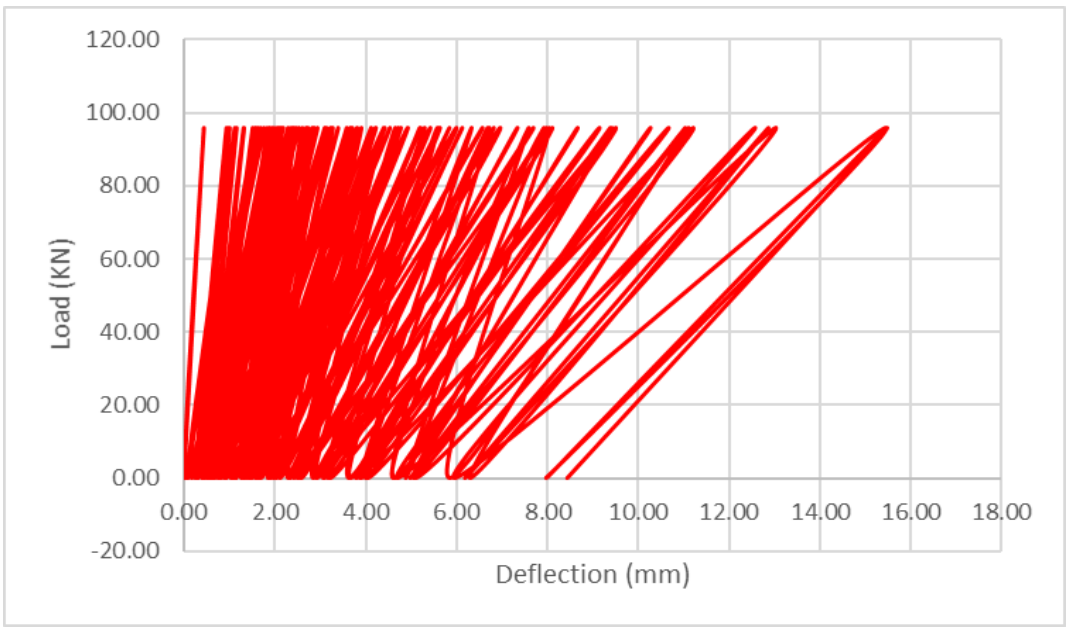

Figure 5.23: load deflection diagram of specimen A-MCB75

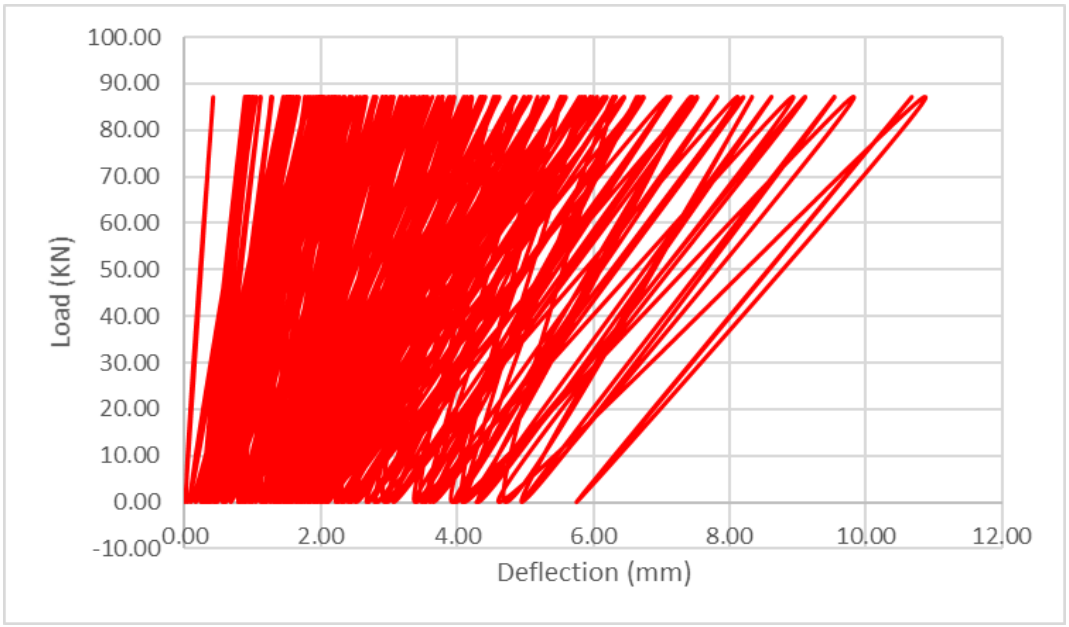

Figure 5.24: load deflection diagram of specimen A-MCB68

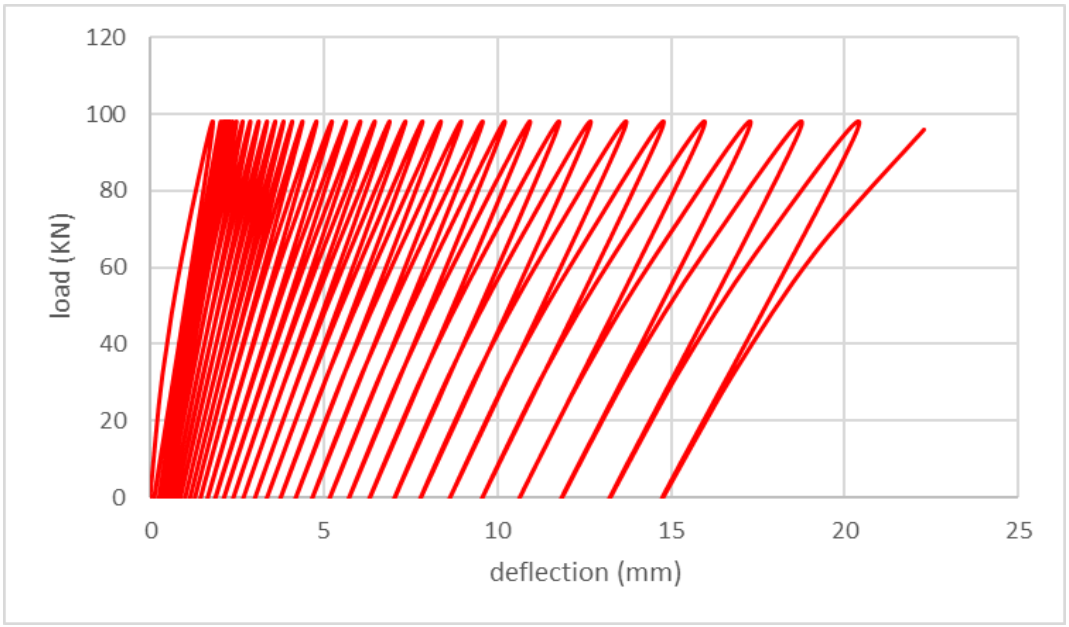

Figure 5.25: load deflection diagram of specimen A-FCB75

5.2 Discussion

5.2.1 Comparison in response of experimental beams

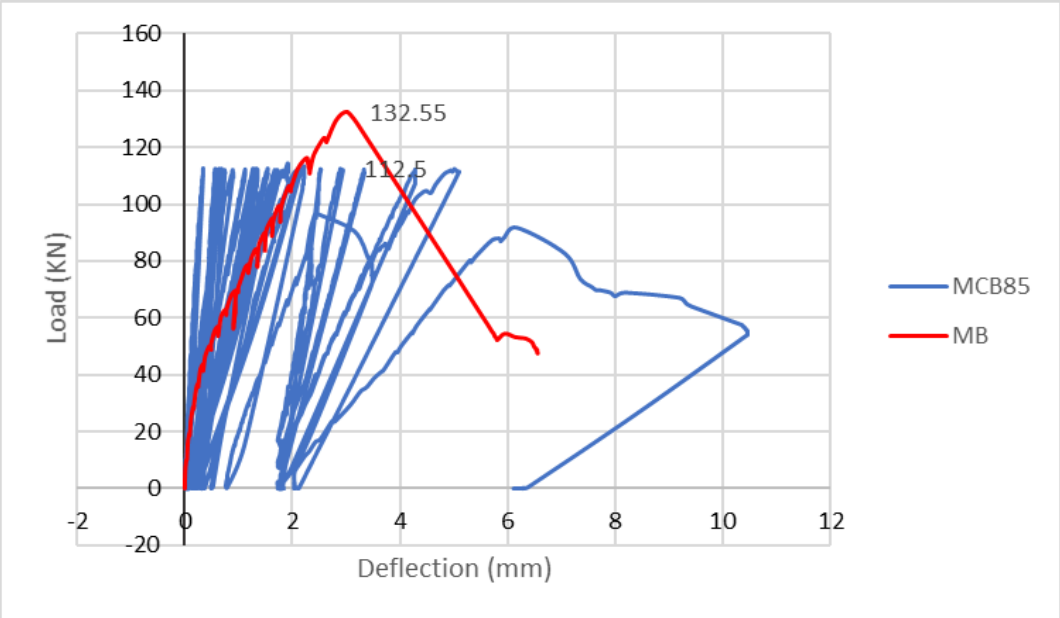

Figure 5.26: comparison between MB and MCB85

The load-deflection responses in Fig 5-26 shows that specimen MCB85 is stiffer than MB. This is mainly because of position of loading. In specimen MCB85 the first loading was applied close to the support, this resulted in a smaller deflection compared to MB which was loaded to failure monotonically at its midspan. The life cycle of the specimen at 85% of its maximum capacity is observed to be 24 cycles.

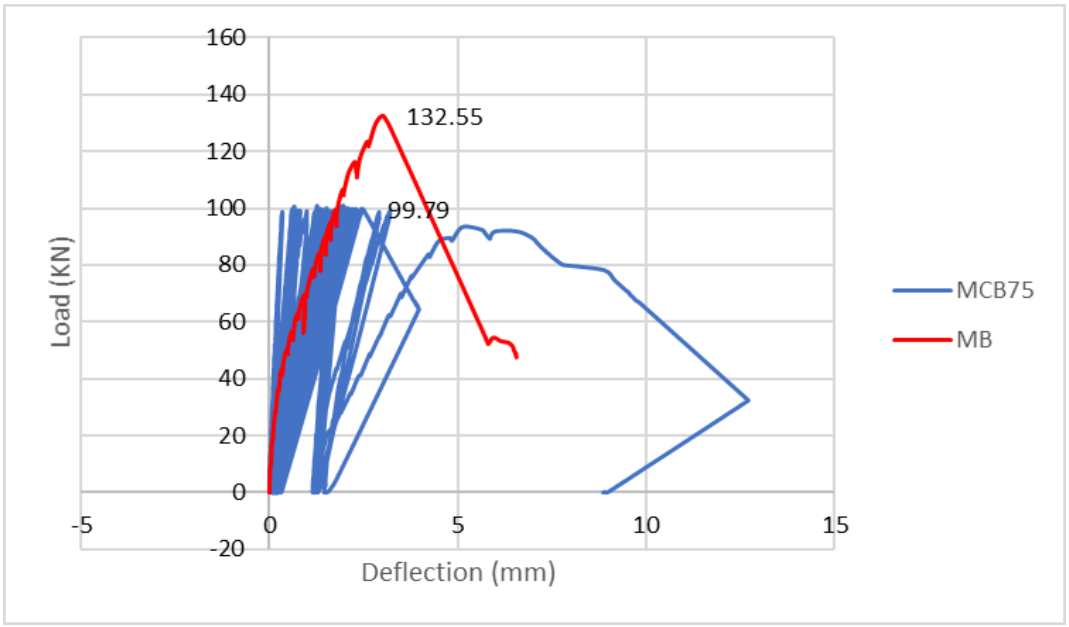

Figure 5.27: comparison between MB and MCB75

The load-deflection response of MCB75 and MB, shows that MCB75 is stiffer than MB. Since, loading on these step-wise moving loaded beams start at 20cm from the left support consequently displacement would be smaller. The life cycle of the specimen at 75% of its maximum capacity is observed to be 213 cycles.

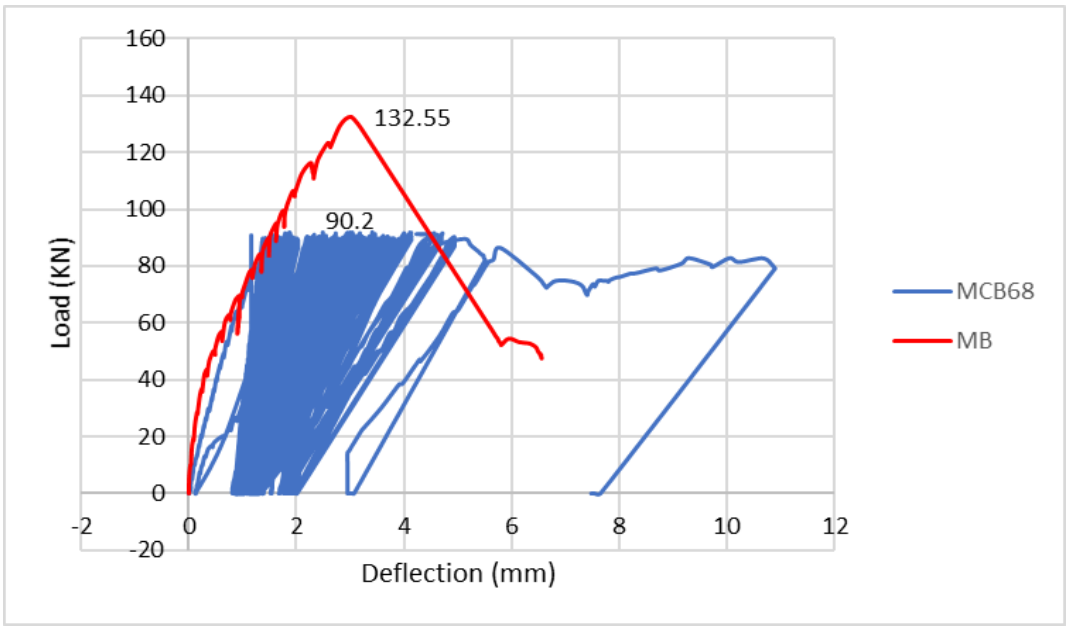

Figure 5.28: comparison between MCB68 and MB

The load-deflection response of specimen MCB68 is very similar to that of specimen MB despite of the loading position, this shows the specimen MCB68 concrete quality or quality of vibration during casting was affected. There by contributing for the beam to have a small stiffness. The life cycle of the specimen at 68% of its maximum capacity is observed to be 165 cycles.

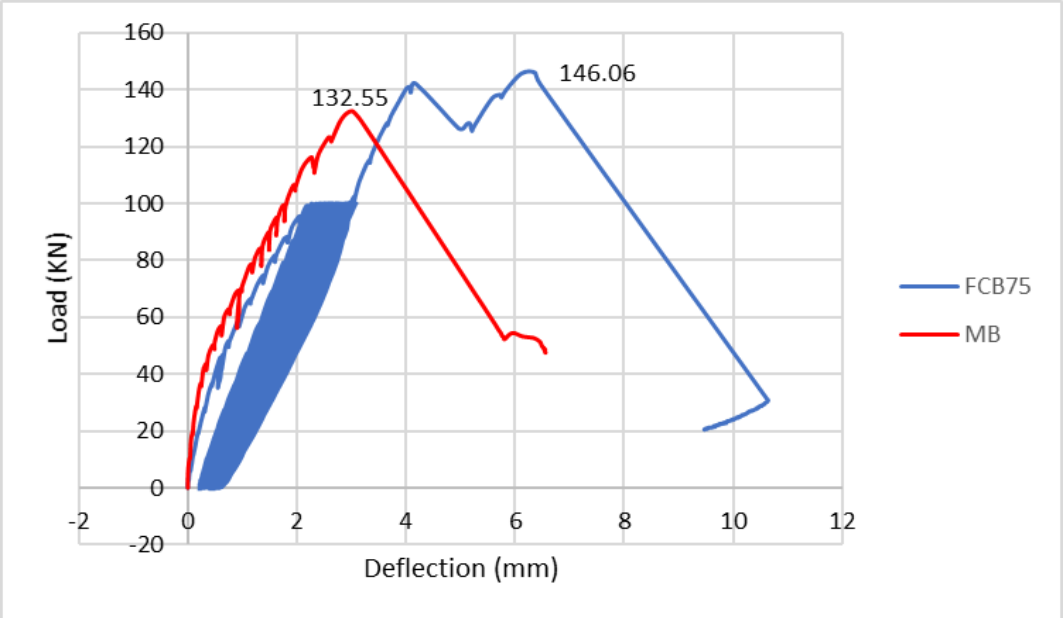

Figure 5.29: comparison between FCB75 and MB

Load-deflection response of specimen FCB75 was very similar with MB in the first cycle of loading. As can be seen from Fig 5.29 the monotonic beam's load-deflection response was observed to be a perfect envelope to the cyclic response of FCB75. After 1000 cycles of fatigue loading, when the beam was loaded monotonically the beam exceeded its maximum capacity by 10.2%. This result agrees with a previous study (Getachew, 2018) In that study when the beam was loaded monotonically to failure after 219 stationary cyclic loading it displayed a higher capacity. The author of this study proposed that fatigue loading might alter diagonal crack path and enhance the shear capacity of beams.

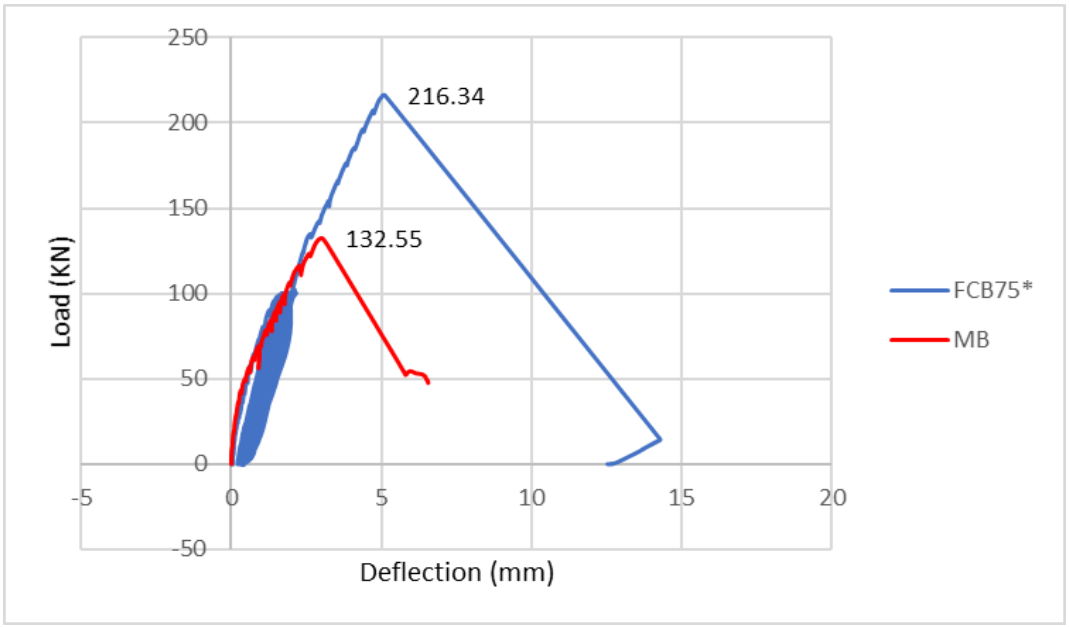

Figure 5.30: comparison between FCB75Cand MB

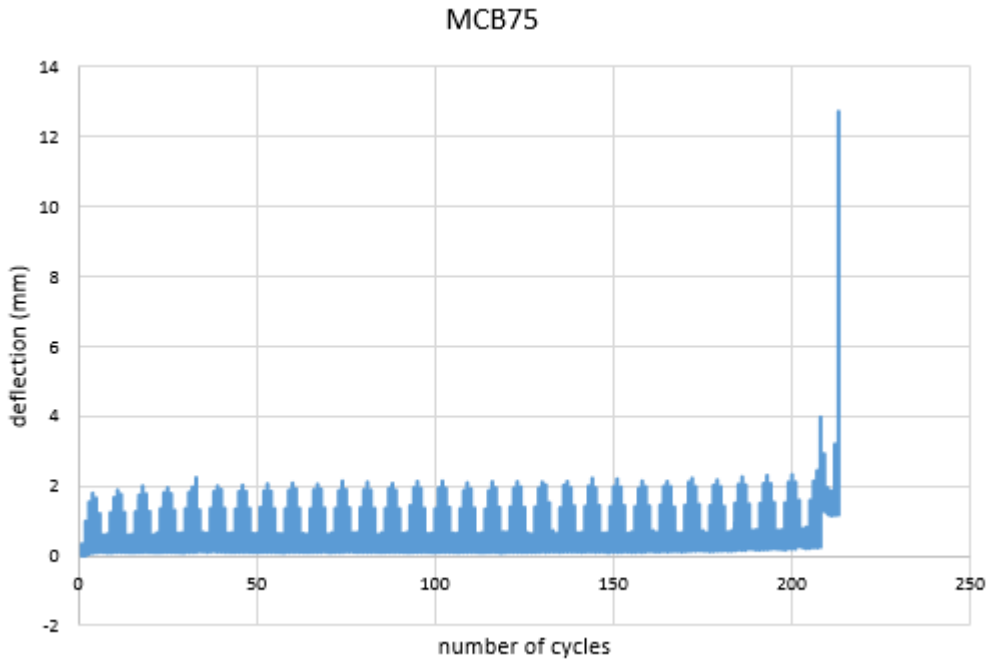

Figure 5.31: Midspan deflection versus number of cycles for MCB75

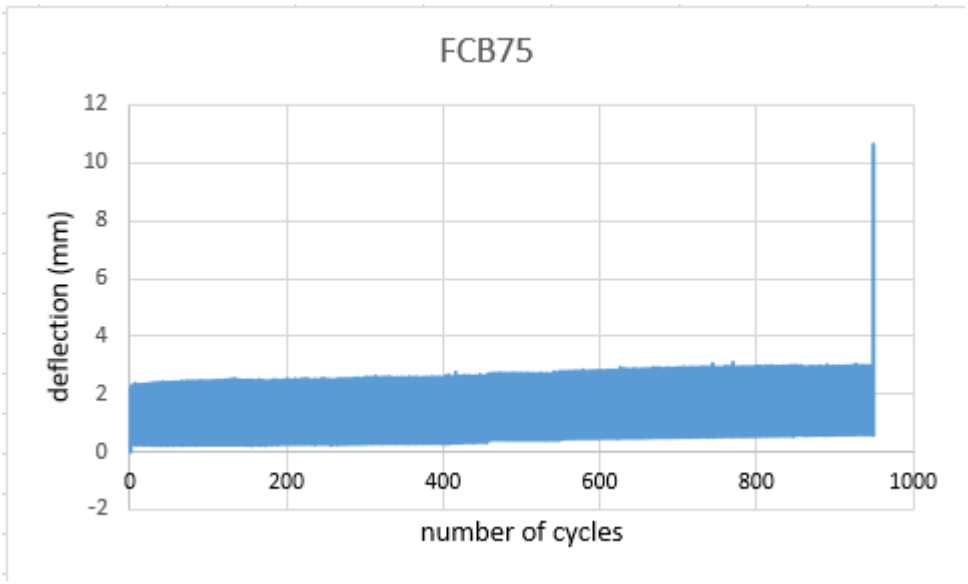

Figure 5.32: Midspan deflection versus number of cycles for FCB75

A midspan deflection of 3.95 mm was recorded at the 208th cycles for the case of MCB75 prior to failure. Which is more than the deflection of the monotonic beam (3.02 mm) at peak load. After five more cycles specimen MCB75 failed in shear having reached a maximum deflection of 12.72 mm. The deflection at the 208th cycle is 1.31 times that of the monotonic beam (MB) at peak load. This shows accumulation of damage prior to failure by MCB75. FCB75 displayed a steady increase in deflection with increasing number of cycles showing increasing damage with increasing number of cycles. However, rate of deflection increase in this beam is much lower than MCB75 indicating that fixed cyclic load has a less damaging effect than the step-wise moving load.

5.2.2 Comparison in response of analytical beams

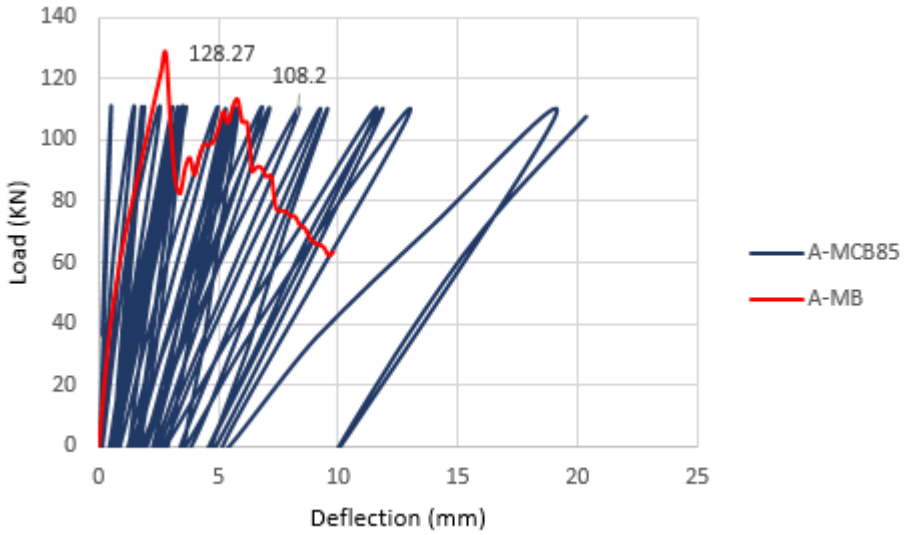

Figure 5.33: comparison between A-MB and A-MCB85

The load-deflection responses in Fig 5-33 shows that specimen A-MCB85 is stiffer than A-MB. This is mainly because of position of loading. In specimen A-MCB85 the first loading was applied close to the support, this resulted in a smaller deflection compared to A-MB which was loaded to failure monotonically at its midspan. The life cycle of the specimen at 85% of its maximum capacity is observed to be 26 cycles.

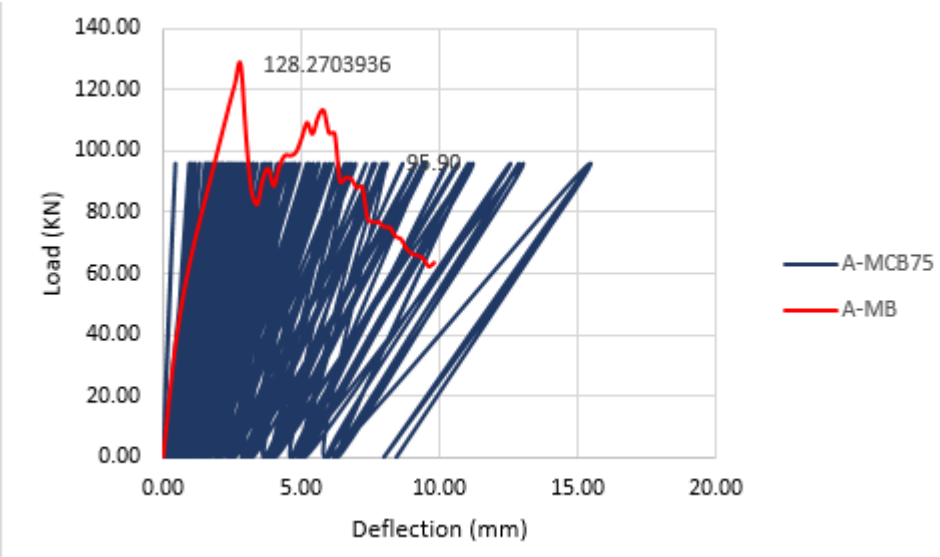

Figure 5.34: comparison between A-MB and A-MCB75

The load-deflection response of A-MCB75 and A-MB, shows that A-MCB75 is stiffer than A-MB. Since, loading on these step-wise moving loaded beams start at 20cm from the left support consequently displacement would be smaller. The life cycle of the specimen at 75% of its maximum capacity is observed to be 120 cycles.

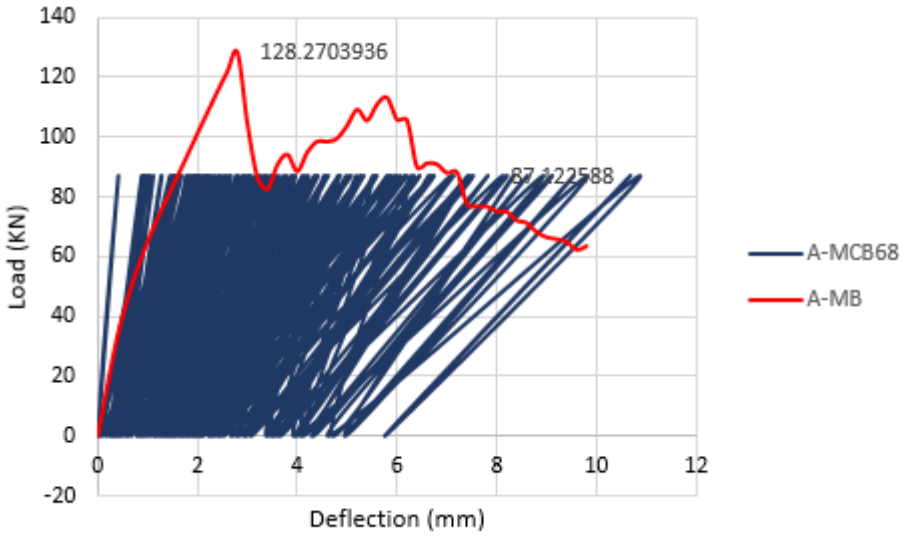

Figure 5.35: comparison between A-MCB68 and A-MB

The load-deflection response of A-MCB68 and A-MB, shows that A-MCB68 is stiffer than A-MB. Since, loading on these step-wise moving loaded beams start at 20cm from the left support consequently displacement would be smaller. The life cycle of the specimen at 68% of its maximum capacity is observed to be 195 cycles.

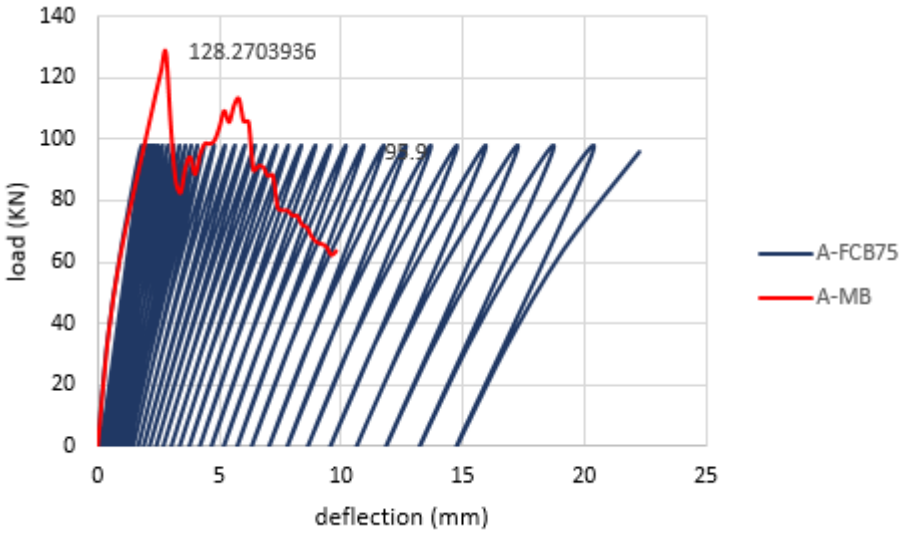

Figure 5.36: comparison between A-FCB75 and A-MB

Load-deflection response of specimen A-FCB75 was very similar with A-MB in the first cycle of loading since in both beams loading started at the mid span unlike the other beams. The life cycle of the specimen at 75% of its maximum capacity is observed to be 1413 cycles. This beam failed after 1413 cycles of loding, and this result do not deviate much from a previous study on RC beam subjected to a moving cyclic load and stationary pulsating load with 75% of its capacity, the beam failed after 1600+ cycles of loading. (Gebreyouhannes & Suryanto, 2019)

5.2.3 Comparison between experimental and analytical results

The analytical simulation result for the monotonic loading shows a close agreement in terms of initial stiffness, maximum capacity, crack pattern and mode of failure to that of the experiment. For the case of moving cyclic loading, the prediction of fatigue life by analytical simulation also gave a close result with the experimental results. However, the analytical simulation shows slightly larger residual deflection from cycle to cycle compared to the experimental tests.

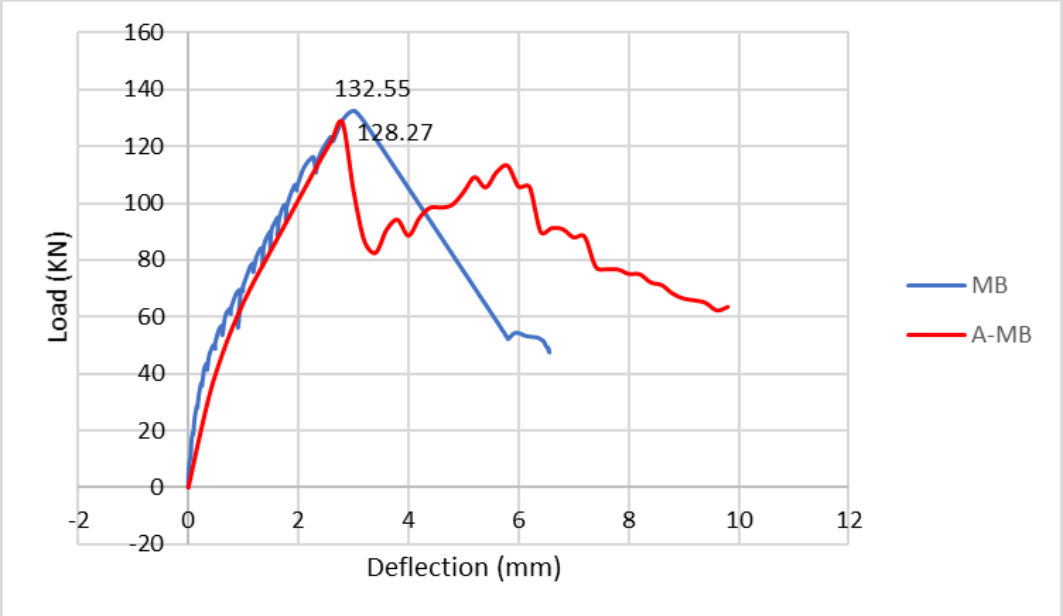

Figure 5.37: comparison between MB and A-MB

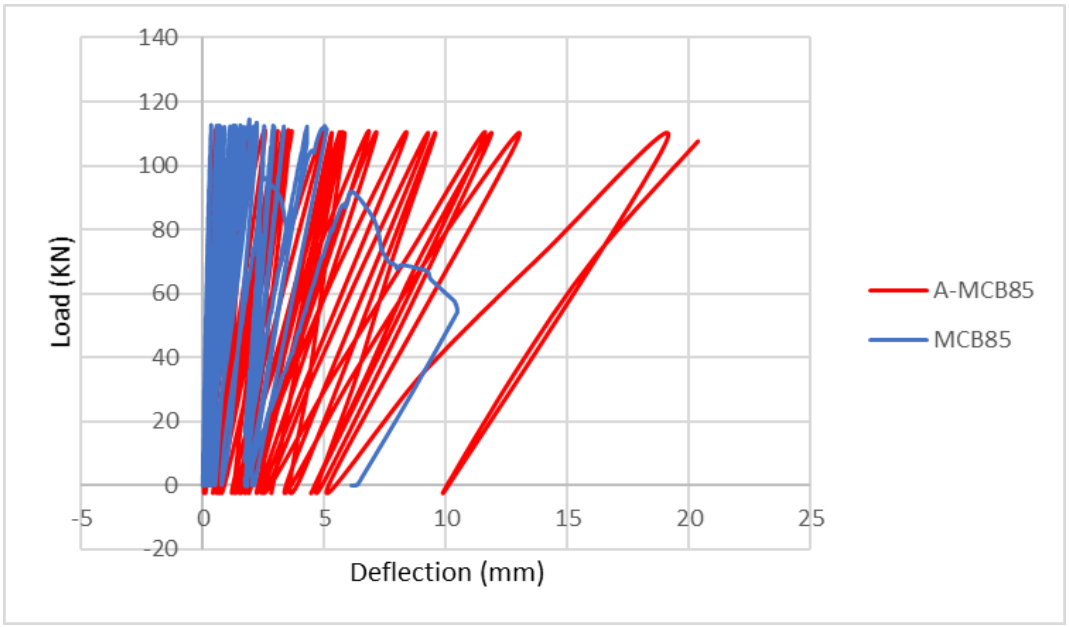

Figure 5.38: comparison between MCB85 and A-MCB85

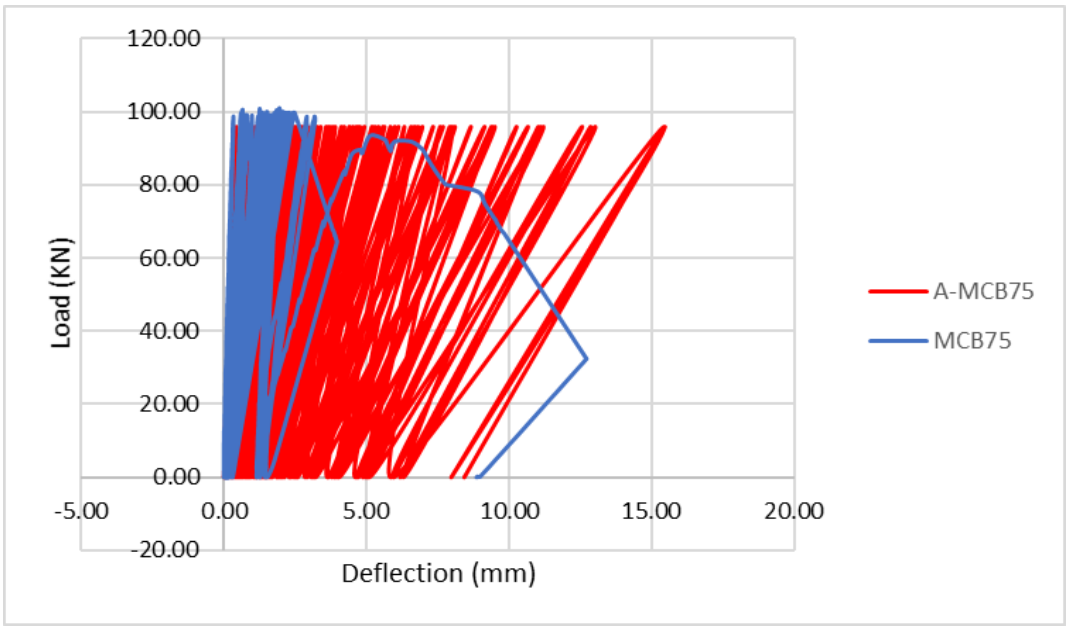

Figure 5.39: comparison between MCB75 and A-MCB75

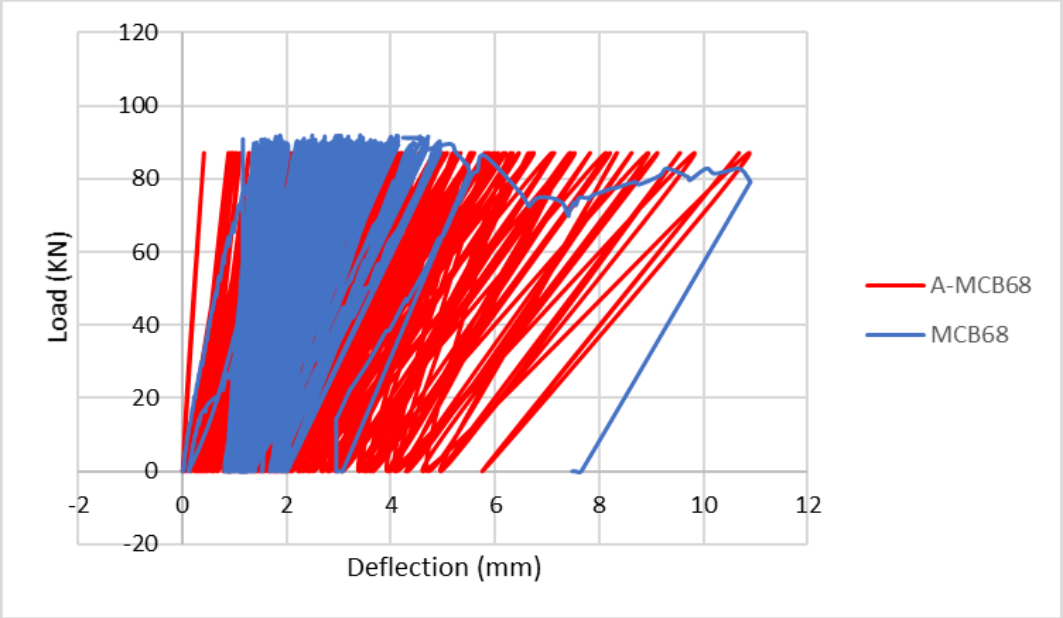

Figure 5.40: comparison between MCB68 and A-MCB68

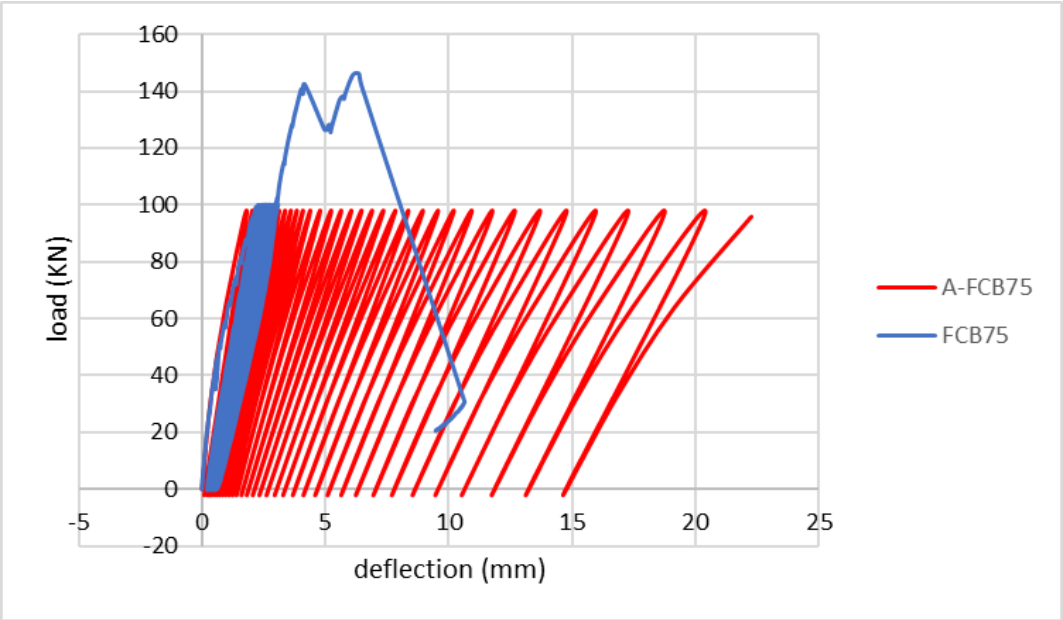

Figure 5.41: comparison between FCB75 and A-FCB75

In specimen MCB85 and MCB68 the analytical simulation on DUCOM-COM3D gave almost exact fatigue life. For the case of specimen MCB75 the analytical simulation slightly underestimated the fatigue life of the concrete. In specimen FCB75 the experiment was loaded monotonically to failure after 1000 cycles and the response during these cycles

was confirmed by the analytical simulation and the stiffness degradation is observed to be very similar.

5.2.4 Diagonal crack pattern

Under fatigue loading, since the beam is continuously being loaded and unloaded the top section of the beam is under compression which makes it difficult for the inclined cracks to progress into the compression zone. Therefore, the major diagonal cracks are more horizontal than that of the beams loaded statically. In specimen MCB85 as it can be shown in Fig 5.43 below that the inclination of the major diagonal crack is less than 20^{o} which is the angle of inclination of specimen MB. For specimen MCB75 and MCB68 this cannot be true. And it might be due to the nature of loading condition. In fatigue loading cracks takes place and damage starts to accumulate on the most damaged section of the beam. So, for the cases of MCB75 and MCB68 the critical cracks took place not towards the mid span like specimen MB and MCB85. The diagonal cracks of specimen MCB75 and MCB68 extended toward loading point C and B respectively as shown in Fig 5.45 and Fig 5.46. Therefore, this would make the inclination of the major diagonal cracks to be more than the monotonic beam.

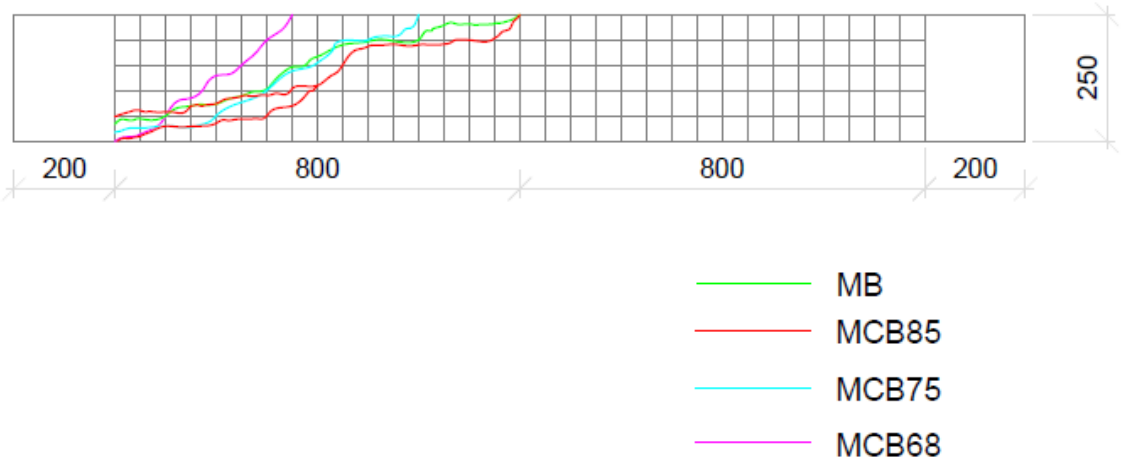

Figure 5.42: Diagonal crack paths of specimen MB, MCB85, MCB75 and MCB68

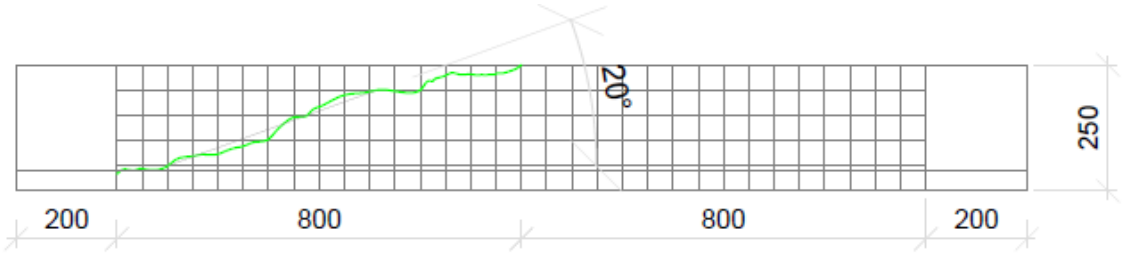

Figure 5.43: Diagonal crack path of specimen MB

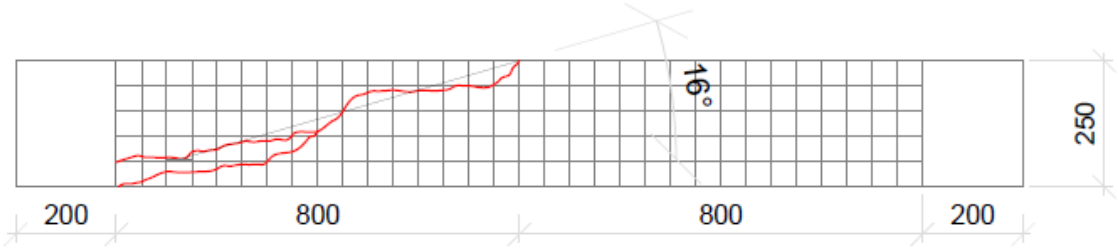

Figure 5.44: Diagonal crack paths of specimen MCB85

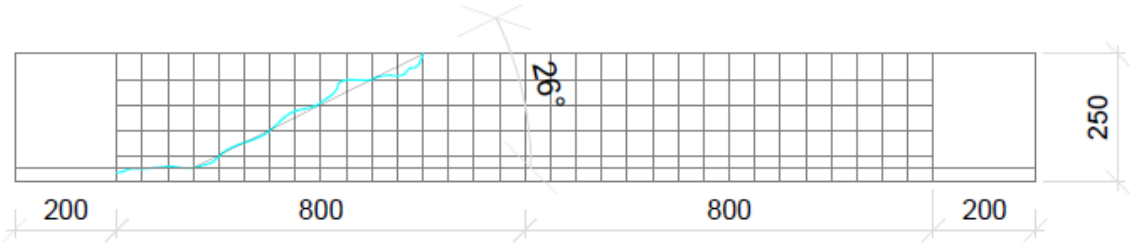

Figure 5.45: Diagonal crack paths of specimen MCB75

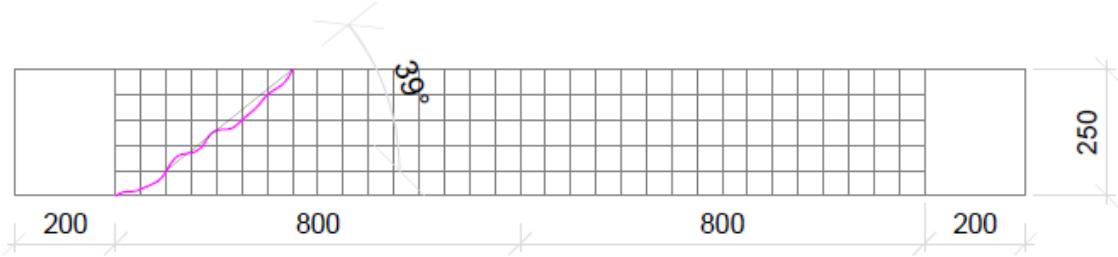

Figure 5.46: Diagonal crack paths of specimen MCB68

5.2.5 S-N curve

In high-cycle fatigue situations, materials performance is commonly characterized by an S-N curve, also known as the Wohler curve. The S-N curves are showing the relation between constant stress amplitude to the material and the number of cycles that leads to failure. In order to obtain the curve, each of the tested specimens is exposed to a cyclic loading with constant amplitude. Then the number of cycles until failure in the specimen is observed. The logarithm of the number of load cycles to failure, N, at the specific stress level is plotted in the diagram. Fatigue analysis was done for all the step wise moving loaded beam analytically by DuCOM-COM3D with 90%, 85%, 80%, 75% and 68% maximum amplitude of their monotonic capacity. In the figure below progress of mid-span deflection with number of cycles is shown. Increase of mid span deflection with increase in number of cycles stipulates for damage progress and strength degradation.

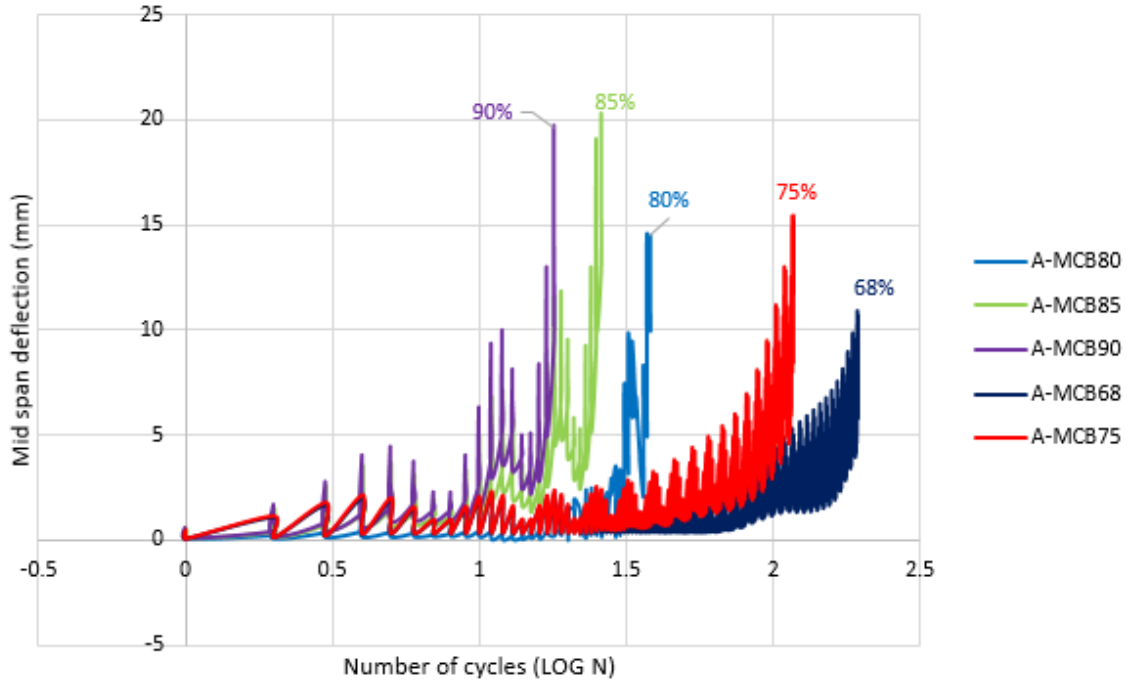

Figure 5.47: deflection-number of cycle relation

A relation between number of cycles to failure and maximum stress for the step-wise moving loading is expressed by the following formula.

$$\frac{V_{max}}{V_{cu}} = 1 - 0.1354logN$$

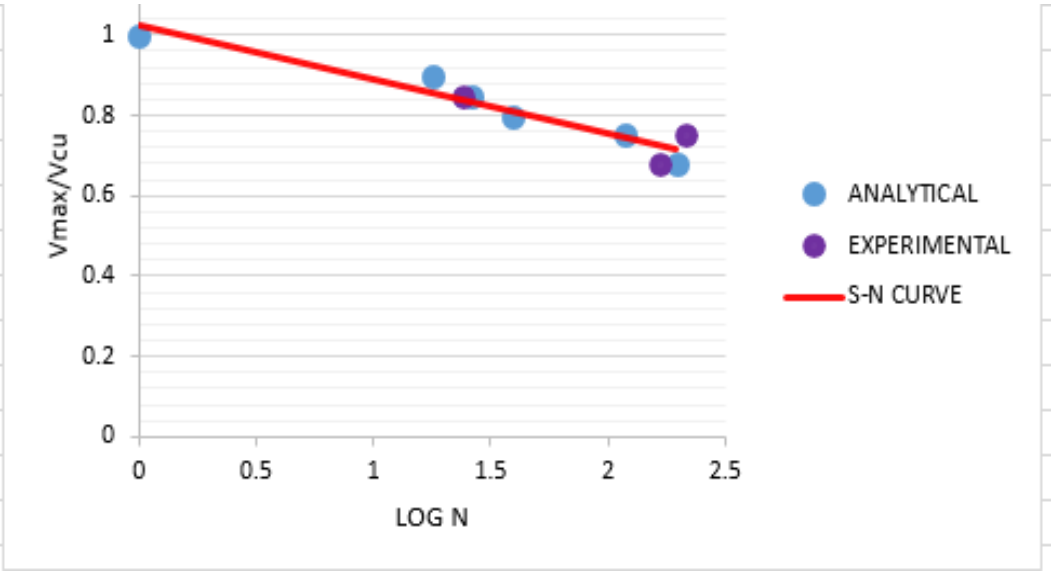

Figure 5.48: S-N diagram for moving cyclic loaded beams

CHAPTER 6 CONCLUSION AND RECCOMENDATION

6.1 Conclusion

In this study the shear fatigue behavior of beams under moving loads was investigated through experimental tests on six shear critical beams, and analytical simulation was also carried out by FEA software DuCOM-COM3D. The following conclusions have been drawn from the findings of the study.

- Step wise moving load causes faster shear strength degradation compared to fixed pulsating load. Rate of beam deflection is higher in moving loads because the stress ratio varies with the movement of the load. This can be clearly seen from the fatigue life of specimens MCB75 and FCB75.
- Maximum and residual deflections of the beams increase with number of load cycles in step wise moving loads which shows higher damage accumulation more than that of fixed pulsating load. This can be clearly seen from the fatigue life of specimens A-MCB85, A-MCB75 and A-MCB68.
- All 3 kinds of loading conditions resulted a diagonal shear cracks with a unique crack pattern. The nature of crack propagation under fatigue loading (Step-wise cyclic loading) is different from the monotonic loading condition. In Specimen MCB85 the major diagonal cracks are more horizontal than that of specimen MB.
- Shear tension failure was observed in all of the beams. Flexural cracks were formed in the first cycles along the span. Then extensions of these cracks were seen at different cycles. Diagonal cracks were then developed and propagated into the compression zone. Splitting cracks along the bottom reinforcements were also observed. Crushing of the concrete in the compression zone adjacent to point of load application was also observed.
- Shear fatigue failure is reached not after the formation of diagonal cracks but after the final shear failure. Thus, brittle shear failure can be avoided if diagonal cracks are detected early.

6.2 Recommendation

In highway bridges, the loads of moving vehicles can cause fatigue damage accumulation of the structures. Overloading in highway bridges can reduce the fatigue life of structures. Avoiding overloading in RC bridges and monitoring fatigue damages for maintenance purpose is recommended.

Further research ideas related to this thesis: -

- Due to the limited ability of the hydraulic actuator the maximum load that can be applied was 300KN. This made the author not to incorporate RC beams with stirrups. But for future studies shear fatigue behavior of RC beams with web reinforcements shall be studied by applying different amplitudes of fatigue loading.
- Effect of shear force to capacity ratio on shear fatigue behavior should be briefly investigated experimentally by locating the critical locations for different RC beams.
- Fatigue of reinforcements in RC beams also occurs in cyclic loadings of RC structures. It can be studied by applying step wise moving loads.

REFERENCES

Ahsan, R. (2016). *Fatigue in Concrete Structures*.

Bachman, P. M., Kreger, M. E., & Breen, J. E. (1987). *Fatigue Strength of Posttensioned Concrete*. *3*.

Day, K. W., Hollon, G. W., Lee, S. H., Pierce, J. S., Popovics, S., Robinson, H. C., Rose, J. H., Scherocman, J. A., Southworth, G. B., Spamer, A. B., Taylor, M. A., Weber, J. W., Ii, D. J. W., Barton, S. G., Bell, L. W., Carter, A. C., Conrey, M. T., & Bell, L. W. (2002). *Standard Practice for Selecting Proportions for Normal , Heavyweight , and Mass Concrete (ACI 211 . 1-91). Reapproved*, 1–38.

EN1992-1-1. (2004). *Eurocode 2: Design of concrete structures - Part 1-1: General rules and rules for buildings*.

Gallego, J. M., Zanuy, C., & Albajar, L. (2014). Shear fatigue behaviour of reinforced concrete elements without shear reinforcement. *Engineering Structures*, *79*, 45–57. https://doi.org/10.1016/j.engstruct.2014.08.005

Gebreyouhannes, E., Chijiwa, N., Fujiyama, C., & Maekawa, K. (2008). Shear fatigue simulation of RC beams subjected to fixed pulsating and moving loads. *Journal of Advanced Concrete Technology*, *6*(1), 215–226. https://doi.org/10.3151/jact.6.215

Gebreyouhannes, E., & Suryanto, B. (2019). Investigating the Mechanism of Shear Fatigue in Reinforced Concrete Beams subjected to Pulsating and Moving Loads using Digital Image Correlation. *Civil Engineering Dimension*, *21*(1), 6–12. https://doi.org/10.9744/ced.21.1.6-12

Getachew, T. (2018). *"Fatigue behavior of shear-critical Reinforced Concrete beams."*

Higai, T. (1983). *FUNDAMENTAL STUDY ON SHEAR FAILURE OF REINFORCED CONCRETE BEAMS*. *279*.

Kawaguchi, M., Yaginuma, Y., & R, V. (1990). *EXPERIMENTS ON FATIGUE STRENGTH OF RC MODEL BEAMS UNDER A RUNNING LOAD*. *269*(420), 269–277.

Maekawa, K., & Mishima, T. (2002). *Shear Failure and Numerical Performance Evaluation of RC Beam Members Made With High-Strength Materials*. *697*, 227–252.

Maekawa, K., Toongoenthong, K., Gebreyouhannes, E., & Kishi, T. (2006). Direct path-integral scheme for fatigue simulation of reinforced concrete in shear. *Journal of Advanced Concrete Technology*, *4*(1), 159–177. https://doi.org/10.3151/jact.4.159

Naik, T. R. (1993). *Fatigue Behavior of Plain Concrete Made With or Without Fly Ash*.

ANNEX

MATERIAL TEST AND MIX DESIGN OF CONCRETE

1 Fine aggregate

1.1. Basic properties

No.	Test description		Test result
1	Silt content		1.67%
2	Moisture content		1.57%
3	Absorption capacity		3.09%
4	Finesse modulus		2.83%
5	Unit weight		1574Kg/m^3
6	Specific gravity	Bulk	2.487
		Bulk (SSD)	2.564
		Apparent	2.69

1.2. Particle size distribution

Sieve size (mm)	Percent passing (%)	ASTM C 33 Standard passing range (%)
9.5	100	100
4.75	100	95-100
2.36	93	80-100
1.18	75	55-85
0.6	39	25-60
0.3	8	5-30
0.15	2	0-10
Pan	-	0

2. Coarse aggregate

2.1. Basic properties

No.	Test description		Test result
1	Nominal size		25mm
2	Moisture content		1.27%
3	Absorption capacity		1.52%
4	Unit weight		1626.01Kg/m^3
5	Specific gravity	Bulk	2.62
		Bulk (SSD)	2.65
		Apparent	2.72

2.2. Particle size distribution

Sieve size (mm)	Percent passing (%)	ASTM C 33 Standard passing range (%)
37.5	100	100
25	77.17	90-100
19	49.9	40-85
12.5	16.7	10-40
9.5	7.4	0-15
4.75	0.2	0-5
Pan	0	0

Concrete Mix Design According to ACI and Binary Method

Target of compressive strength =C20/25 MPa (C-25)

28-day Cylindrical Strength fck,cylinder=20 Mpa

28-day Cubic Compressive Strength fck,cube=25 MPa

Materials parameters are described as follow:

Cement; specific gravity= 3.15

Bulk specific gravity C.A=2.62

SSD specific gravity C.A=2.65

Apparent specific gravity C.A=2.72

Compacted unit weight C.A=1626.01 kg/m³

Moisture content of C.A = 1.27%

Absorption capacity of C.A = 1.52%

Bulk specific gravity F.A =2.49

SSD specific gravity F.A=2.564

Apparent specific gravity C.A=2.69

Fines modulus F.A=2.83

Moisture content of F.A = 1.57%

Absorption capacity of F.A = 3.09%

Unit weight F.A=1574 kg/m³

Density of water=1000 kg/m3

- **Step 1**: choice of slump

  From ACI mix design table A1.5.3.1 (Day et al., 2002)

  For beams slump is 25mm – 100mm. take 75mm.

- **Step 2**: choice of nominal maximum aggregate size

  The nominal maximum aggregate size is 25mm.

- **Step 3:** estimation of mixing water and air content

  From ACI mix design Table A1.5.3.3 The estimated mixing water for a slump of 75 to 100 mm in non-air-entrained concrete made with 25 mm aggregate is found to be 190 kg/m3
  Entrapped air is 2%.
  Assumption of sand to aggregate ratio according to binary method 0.45 for 25MPa-33Mpa.

- **Step 4**: Selection of water-cement ratio
  From ACI mix Design table A1.5.3.4 w/c ratio for non-air entrained concrete with cubic compressive strength of 28MPa is 0.579.

- **Step 5**: calculation of cement content

  The required cement content is 190/0.579 = 328.152 kg/m³

- **Step 6**: estimation of coarse aggregate content

  Volume of water = 190 kg/m3 = 0.19*1000=190 liter
  Volume of air = 2%=0.02*1000=20 liter
  Volume of cement = Vc= 328.152*1000/3.15*1000 = 104.175l

$$\frac{V_S}{V_G + V_S} = 0.45$$

$$0.55Vs=0.45Vs$$

  Vtotal = 1000l=Vw+Vc+Vs+Vg+Va

$$1000l= 190l + 104.175l + 20l + Vs + 1.22Vs$$

$$Vs = 308.621l$$

$$Vg = 377.204l$$

$$Ms = 308.621*2.564=791.304\ Kg$$

$$Mg= 377.204*2.65=999.591\ Kg$$

  The required dry mass is = 0.677 x 1626.01 = 1084.55 kg.

Final result

Average cylinderical strength	28MPa
OPC cement	328.152kg/m3
Maximum aggregate size	25mm
water	190kg/m3
Coarse aggregate	999.591 kg/m3
Fine aggregate	791.304 kg/m3
Water cement ratio	0.579